The Astronomical Journal, 139:519–539, 2010 February doi:10.1088/0004-6256/139/2/519

THE CARNEGIE SUPERNOVA PROJECT: FIRST PHOTOMETRY DATA RELEASE OF LOW-REDSHIFT TYPE Ia SUPERNOVAE*

Carlos Contreras[1], Mario Hamuy[2], M. M. Phillips[1], Gastón Folatelli[1,2], Nicholas B. Suntzeff[3,4], S. E. Persson[5], Maximilian Stritzinger[1,6], Luis Boldt[1], Sergio González[1], Wojtek Krzeminski[1], Nidia Morrell[1], Miguel Roth[1], Francisco Salgado[1,2], María José Maureira[2], Christopher R. Burns[5], W. L. Freedman[5], Barry F. Madore[5,7], David Murphy[5], Pamela Wyatt[7], Weidong Li[8], and Alexei V. Filippenko[8]
[1] Las Campanas Observatory, Carnegie Observatories, Casilla 601, La Serena, Chile
[2] Departamento de Astronomía, Universidad de Chile, Casilla 36-D, Santiago, Chile
[3] Physics Department, Texas A&M University, College Station, TX 77843-4242, USA
[4] Mitchell Institute for Fundamental Physics and Astronomy, Texas A&M University, College Station, TX 77843-4242, USA
[5] Observatories of the Carnegie Institution of Washington, 813 Santa Barbara St., Pasadena, CA 91101, USA
[6] Dark Cosmology Centre, Niels Bohr Institute, University of Copenhagen, Juliane Maries Vej 30, 2100 Copenhagen Ø, Denmark
[7] Infrared Processing and Analysis Center, Caltech/Jet Propulsion Laboratory, Pasadena, CA 91125, USA
[8] Department of Astronomy, University of California, Berkeley, CA 94720-3411, USA
Received 2009 May 20; accepted 2009 October 31; published 2010 January 12

ABSTRACT

The Carnegie Supernova Project (CSP) is a five-year survey being carried out at the Las Campanas Observatory to obtain high-quality light curves of ∼100 low-redshift Type Ia supernovae (SNe Ia) in a well-defined photometric system. Here we present the first release of photometric data that contains the optical light curves of 35 SNe Ia, and near-infrared light curves for a subset of 25 events. The data comprise 5559 optical (*ugriBV*) and 1043 near-infrared ($YJHK_s$) data points in the natural system of the Swope telescope. Twenty-eight SNe have pre-maximum data, and for 15 of these, the observations begin at least 5 days before *B* maximum. This is one of the most accurate data sets of low-redshift SNe Ia published to date. When completed, the CSP data set will constitute a fundamental reference for precise determinations of cosmological parameters, and serve as a rich resource for comparison with models of SNe Ia.

Key words: galaxies: distances and redshifts – supernovae: general

Online-only material: color figures, figure set, machine-readable and VO tables

1. INTRODUCTION

The observation that the expansion rate of the universe is currently accelerating is arguably one of the most profound discoveries in modern astrophysics. The first direct evidence of this phenomenon was provided a decade ago by the Hubble diagram of high-redshift Type Ia supernovae (SNe Ia; Riess et al. 1998; Perlmutter et al. 1999). Since then, a wealth of data obtained from surveys of nearby and distant SNe Ia has confirmed this conclusion, as have other methods such as the X-ray cluster distances (e.g., Allen et al. 2007) and the late-time-integrated Sachs–Wolfe effect using cosmic microwave background radiation observations (e.g., Giannantonio et al. 2008). These findings suggest that a new form of energy permeates the universe, or that the theory of general relativity breaks down on cosmological scales.

Today, the major challenge is to determine the nature of this mysterious energy (commonly referred to as "dark energy") by measuring its equation-of-state parameter, $w = P/(\rho c^2)$, and the corresponding time derivative $\dot{w}$. SNe Ia are playing an essential role in the endeavor to measure w. Both the SN Legacy Survey (Astier et al. 2006) and the ESSENCE project (Wood-Vasey et al. 2007) have recently provided independent constraints on w that favor a cosmological constant ($w = -1$). The determination of $\dot{w}$, however, will require new and extensive samples of both low- and high-redshift SNe Ia with systematic errors below 1%–2%. This will require the construction of a database of low-redshift light curves with excellent photometric precision and temporal coverage.

The pioneering work of producing such a low-redshift sample of SNe Ia was carried out by the Calán/Tololo Survey, which published *BV RI* light curves of 29 events (Hamuy et al. 1996). This is the local sample that was used by Riess et al. (1998) and Perlmutter et al. (1999) to detect the accelerating expansion of the universe. In 1999, the CfA Supernova Group released a set of 22 *BV RI* light curves (Riess et al. 1999). Subsequently, this group has published *U BV RI* light curves of 44 events (Jha et al. 2006), and *U BV RIr′i′* light curves of another 185 (Hicken et al. 2009). Other significant samples of nearby SNe Ia are being produced by the Lick Observatory Supernova Search (LOSS; Filippenko et al. 2001; Filippenko 2005, A. Filippenko et al. 2010, in preparation) and the Nearby Supernova Factory (Aldering et al. 2002). In addition, the SDSS-II Supernova Survey (Frieman et al. 2008) has obtained $u'g'r'i'z'$ light curves of a sample of ∼500 spectroscopically confirmed SNe Ia in the redshift range of $0.05 < z < 0.35$.

In 2004 September, the Carnegie Supernova Project (hereafter CSP) began a five-year program to obtain densely sampled optical *and* near-infrared light curves of ∼100 nearby SNe Ia. The overriding goal has been to obtain the highest possible precision in a stable, well-understood photometric system. An additional objective is to use the broad wavelength leverage afforded by these observations to set stringent constraints on the properties of host-galaxy extinction (see Folatelli et al. 2010). In this paper, we present final photometry of the first 35 SNe Ia observed in the years 2004–2006. This data set consists of optical ($u'g'r'i'BV$) light curves of all 35 SNe, and near-infrared ($YJHK_s$) light curves for a subset of 25. In total, 5559 optical and 1043 near-infrared measurements were obtained at a typical precision of 0.01–0.03 mag, making this one of the most

* This paper includes data gathered with the 6.5 m Magellan Telescopes located at the Las Campanas Observatory, Chile.

homogeneous and accurate sets of nearby SN Ia light curves yet obtained. A distinguishing aspect of the CSP is the quantity and quality of the near-infrared photometry, which is matched only by the recently published PAIRITEL results (Wood-Vasey et al. 2008).

Previously, Hamuy et al. (2006, hereafter H06) gave a detailed description of the CSP observing methodology and data reduction procedures, and showed several examples of light curves obtained during the first campaign. In a second paper, Folatelli et al. (2006) reported on the unique Type Ib SN 2005bf, while the third CSP paper presented a detailed analysis of the peculiar Type Ia SN 2005hk (Phillips et al. 2007). A fourth paper on the distance to the Antennae Galaxies (NGC 4038/39) based on the Type Ia SN 2007sr was presented by Schweizer et al. (2008). CSP photometry has also been included in case studies of the subluminous Type Ia SN 2005bl (Taubenberger et al. 2008) and the Type Ia/IIn SN 2005gj (Prieto et al. 2007). Most recently, Stritzinger et al. (2009) published a comprehensive study on the Type Ib SN 2007Y.

The organization of this paper is as follows. Section 2 describes the observing and basic data reduction procedures, Section 3 reviews the establishment of the local photometric sequences, Section 4 gives details of the measurement and calibration of the SN photometry, and Section 5 presents the final light curves. In two Appendices, we present our most up-to-date information on the sensitivity functions of our $u'g'r'i'BV$ bandpasses, and near-infrared photometry of Feige 16 obtained over the course of our observing campaigns which we use to check the validity of our Y-band calibration.

Accompanying this paper are two other papers. The first gives an analysis of the data presented here (Folatelli et al. 2010). The second combines the data of this paper with that of 35 high-redshift SNe Ia, observed in the near-infrared with the Magellan Baade 6.5 m telescope, in order to construct the first rest-frame i-band Hubble diagram out to $z \approx 0.7$ (Freedman et al. 2009).

2. OBSERVATIONS AND BASIC DATA REDUCTIONS

The CSP carries out one nine-month campaign each year from September through May. All the data presented below were obtained during the first three campaigns from 2004 through 2006. In H06, the observing procedures and data reduction techniques were described in detail; below we briefly summarize. Since the publication of H06, the optical photometry reductions have been modified so that the magnitudes of each SN Ia are computed in the *natural* system of the Swope telescope CCD imager. This new approach is discussed in Section 4.2.1.

2.1. Sample Selection

A list of the general properties of the 35 SNe Ia (17, 14, and 4 in the first, second, and third campaigns, respectively) whose light curves are presented in this paper is given in Table 1. This table includes (1) the equatorial coordinates of each SN, (2) the name, morphology, and heliocentric redshift of the host galaxy, (3) the discovery reference, and (4) the discovery group or individual. As is seen, approximately one third of the SNe were discovered by LOSS with the Katzman Automatic Imaging Telescope (KAIT), while the remainder are drawn from a number of sources. In general, the only criteria used by the CSP to select which SN to follow were (1) discovery before or near maximum brightness, and (2) a magnitude no fainter than 18–18.5 at the time of discovery. However, each of the discovery groups or individuals listed in Table 1 employs different search strategies (cadence, depth, target selection, etc.). In a future paper, we plan to explore the possible biases introduced by such a heterogeneous sample. Here, we briefly describe the completeness of the LOSS discoveries and how this relates to Malmquist bias.

LOSS is a targeted search which annually monitors a sample of $\sim 14{,}000$ galaxies (A. Filippenko et al. 2010, in preparation, and references therein). In 2004, the search was deliberately adjusted to include more galaxies south of the celestial equator, to enlarge the potential sample accessible to the CSP. In order to study the completeness of the survey, we constructed an observed luminosity function for LOSS SNe Ia from 56 discoveries within 80 Mpc. Based on this luminosity function, we conclude that LOSS has missed very few SNe Ia in its sample galaxies within $z \leqslant 0.04$. Over most of the observed luminosity range, the expected completeness is $> 80\%$ at $z = 0.04$. Since most of the LOSS galaxies are within 100 Mpc ($z = 0.024$), the actual missing fraction of SNe Ia is quite small.

Hence, a program that follows all of the LOSS SN Ia discoveries should end up with a fairly complete sample, with minimal Malmquist bias. Of course, the CSP is only able to follow those LOSS SNe which are accessible from the southern hemisphere. For these galaxies, which are located at relatively large zenith distances at the Lick Observatory, the completeness is probably somewhat smaller due to the difficulty of the observations (seeing conditions, airmass, etc.). Nevertheless, we expect that Malmquist bias for the subset of the LOSS SNe Ia at $z \leqslant 0.04$ followed by the CSP should be small. Of the 12 LOSS SNe included in Table 1, only one (SN 2005ag) lies at $z > 0.04$.

2.2. Observations

Our follow-up program focuses on SNe discovered by professional and amateur astronomers who report them to the IAU Circulars (IAUC), the IAU Electronic Telegrams (CBET), or occasionally, directly to us via electronic mail. When word arrives of a new candidate, we place it in our follow-up queue. Photometric monitoring is obtained entirely at the Las Campanas Observatory (LCO). The optical follow-up observations are conducted with the SITe3 CCD camera attached to the Swope 1 m telescope, which has been available to the CSP $\sim$250 nights per campaign. During the first campaign, the near-infrared follow-up was carried out solely with the Wide Field Infrared Camera (WIRC) attached to the du Pont 2.5 m Telescope. However, by the start of the second campaign, a new near-infrared camera called RetroCam, built by S.E.P. and D.M. for this program, became available on the Swope telescope. The addition of RetroCam significantly enhanced our ability to obtain detailed YJH-band light curves. Nevertheless, we have continued to use WIRC to observe the fainter targets. In several cases, supplementary imaging has also been performed with the near-infrared imager, PANIC, attached to the Magellan Baade telescope.

In addition to follow-up observations, the du Pont Telescope is used to obtain optical and near-infrared template images of the host galaxies. These templates are used to subtract away the host-galaxy contamination in each of our science images before instrumental magnitudes are computed (see Section 4.1).

Figure 1 presents a mosaic constructed with a V-band image of each SN. In Table 2, the following photometric and spectroscopic information is collected for each SN: (1) an estimate of the decline-rate parameter $\Delta m_{15}(B)$ (Phillips 1993); (2) the number of optical and near-infrared epochs each event was observed; (3) the number of photometric nights that the optical

Table 1
General Properties of the 35 SNe Ia

SN	SN α(2000)	SN δ(2000)	Host Galaxy	Morphology[a]	$z_{\rm helio}$[a]	Discovery Reference	Discovery Group/Individual[b]
2004dt	02:02:12.77	−00:05:51.5	NGC 799	(R')SB(s)a	0.0197	IAUC 8386	LOSS
2004ef	22:42:10.02	+19:59:40.4	UGC 12158	Sb	0.0310	IAUC 8399	Boles; Armstrong
2004eo	20:32:54.19	+09:55:42.7	NGC 6928	SB(s)ab	0.0157	IAUC 8406	Itagaki
2004ey	21:49:07.81	+00:26:39.2	UGC 11816	SB(rs)c	0.0158	IAUC 8419	Tenagra II
2004gc	05:21:49.95	+06:40:33.7	ARP 327 NED04	···	0.0321	IAUC 8442	del Olmo et al. ; Tenagra II
2004gs	08:38:23.18	+17:37:39.8	MCG +03-22-020	S0?	0.0267	IAUC 8453	LOSS
2004gu	12:46:24.72	+11:56:56.1	FGC 175A	···	0.0459	IAUC 8454	ROTSE-III
2005A	02:30:43.25	−02:56:19.8	NGC 958	SB(rs)c	0.0191	IAUC 8459	LOSS
2005M	09:37:32.36	+23:12:02.7	NGC 2930	S?	0.0220	IAUC 8470	Puckett
2005W	01:50:45.77	+21:45:35.4	NGC 691	SA(rs)bc	0.0089	IAUC 8475	Hirose
2005ag	14:56:43.65	+09:19:42.5	···	···	0.0794	IAUC 8484	LOSS
2005al	13:50:00.33	−30:34:34.2	NGC 5304	E+ pec	0.0124	IAUC 8488	BRASS
2005am	09:16:12.47	−16:18:16.0	NGC 2811	SB(rs)a	0.0079	IAUC 8490	Perth
2005be	14:59:32.72	+16:40:11.6	···	···	0.0350	IAUC 8506	Puckett
2005bg	12:17:17.18	+16:22:17.6	MCG +03-31-93	Sab	0.0231	CBET 133	ROTSE-III
2005bl	12:04:12.26	+20:24:24.8	NGC 4059	E	0.0241	IAUC 8512	LOSS; Puckett
2005bo	12:49:41.03	−11:05:47.3	NGC 4708	SA(r)ab pec?	0.0139	CBET 141	Puckett
2005el	05:11:48.72	+05:11:39.4	NGC 1819	SB0	0.0149	CBET 233	LOSS
2005eq	03:08:49.31	−07:01:59.7	MCG −01-09-006	SB(rs)cd?	0.0290	IAUC 8608	LOSS
2005hc	01:56:47.94	−00:12:49.4	MCG +00-06-003	···	0.0459	CBET 259	SDSS II
2005iq	23:58:32.50	−18:42:33.0	MCG −03-01-008	Sa	0.0340	IAUC 8628	LOSS
2005ir	01:16:43.76	+00:47:40.4	···	···	0.0764	CBET 277	SDSS II
2005kc	22:34:07.34	+05:34:06.3	NGC 7311	Sab	0.0151	IAUC 8629	Puckett
2005ke	03:35:04.35	−24:56:38.8	NGC 1371	(R')SAB(r')a	0.0049	IAUC 8630	LOSS
2005ki	10:40:28.22	+09:12:08.4	NGC 3332	(R)SA0	0.0192	IAUC 8632	LOSS
2005lu	02:36:03.71	−17:15:50.0	ESO 545-G038	S.../Irr?	0.0320	IAUC 8645	LOSS
2005na	07:01:36.62	+14:07:59.7	UGC3634	SB(r)a	0.0263	CBET 350	Puckett
2006D	12:52:33.94	−09:46:30.8	MCG −01-33-34	SAB(s)ab pec? H II	0.0085	CBET 362	BRASS
2006X	12:22:53.99	+15:48:33.1	NGC 4321	SAB(s)bc	0.0052	IAUC 8667	Suzuki; CROSS
2006ax	11:24:03.46	−12:17:29.2	NGC 3663	SA(rs)bc pec	0.0167	CBET 435	LOSS
2006bh	22:40:16.10	−66:29:06.3	NGC 7329	SB(r)b	0.0109	CBET 457	Monard
2006eq	21:28:37.13	+01:13:41.5	···	···	0.0495	CBET 611	SDSS II
2006gt	00:56:17.30	−01:37:46.0	J00561810-013732	···	0.0448	CBET 641	ROTSE-III
2006mr	03:22:43.04	−37:12:29.6	NGC1316	SAB	0.0059	CBET 723	Monard
2006py	22:41:42.05	−00:08:12.9	···	···	0.0579	CBET 762	SDSS II

Notes.
[a] Host galaxy morphologies and heliocentric redshifts taken from the NASA/IPAC Extragalactic Database (NED).
[b] References/URLs: LOSS (see Filippenko 2005, and references therein); Tenagra II (http://www.tenagraobservatories.com/Discoveries.htm); ROTSE-III (Quimby 2006)); Puckett (http://www.cometwatch.com); BRASS (http://brass.astrodatabase.net); Perth (Williams 1997); SDSS II (Frieman et al. 2008); CROSS (http://wwww.cortinasetelle.it/snindex.htm)

and near-infrared local sequences were calibrated; and (4) the spectral subtype of each event and the epoch of the spectrum used to make the identification.

Spectral identification was performed using the SuperNova IDentification tool (SNID; Blondin & Tonry 2007). Twenty-six events are identified as normal, four as SN 1991bg-like, two as SN 1991T-like, and one as SN 2006gz-like. The identification of a dozen of the normal subtypes was obtained with spectra sufficiently past maximum that a SN 1991T-like identification cannot be excluded. However, out of these dozen events, only SN 2005lu ($\Delta m_{15}(B) = 0.88 \pm 0.03$) has a B-band decline rate that is similar to that of other SN 1991T-like events, which typically exhibit $\Delta m_{15}(B)$ values of 0.9 or less.

Figure 2 compares our day −3 spectrum of SN 2004gu to similar-epoch spectra of the peculiar SNe 1999ac (Phillips et al. 2006) and 2006gz (Hicken et al. 2007; Maeda et al. 2009). As is evident, SN 2004gu resembled both of these events, but clearly a better overall match is with SN 2006gz. The spectra of SNe 2004gu and 2006gz show an unusually strong Si III line at 4560 Å while the Ca II H&K feature appears to be more prevalent in SN 2004gu. Interestingly, SNe 2004gu and 2006gz have nearly identical decline rates of $\Delta m_{15}(B) \approx 0.70$–$0.80$ mag. Moreover, for a reddening law of $R_V = 1.2$, we compute very similar absolute peak magnitudes of $M_B = -19.63 \pm 0.09$ for SN 2004gu (Folatelli et al. 2010) and $M_B = -19.57 \pm 0.16$ for SN 2006gz (Hicken et al. 2007).

2.3. Data Reduction

Basic data reductions are generally carried out the day following the observation. This allows us to measure preliminary photometry to obtain a prompt estimate of the age and brightness of the SN. This information is particularly useful to help us decide whether or not a new target merits extensive follow-up observations.

The optical images are reduced with the IRAF[9] task CCDPROC. The basic reduction process consists of (1) bias

[9] IRAF is distributed by the National Optical Astronomy Observatories, which are operated by the Association of Universities for Research in Astronomy, Inc., under cooperative agreement with the National Science Foundation.

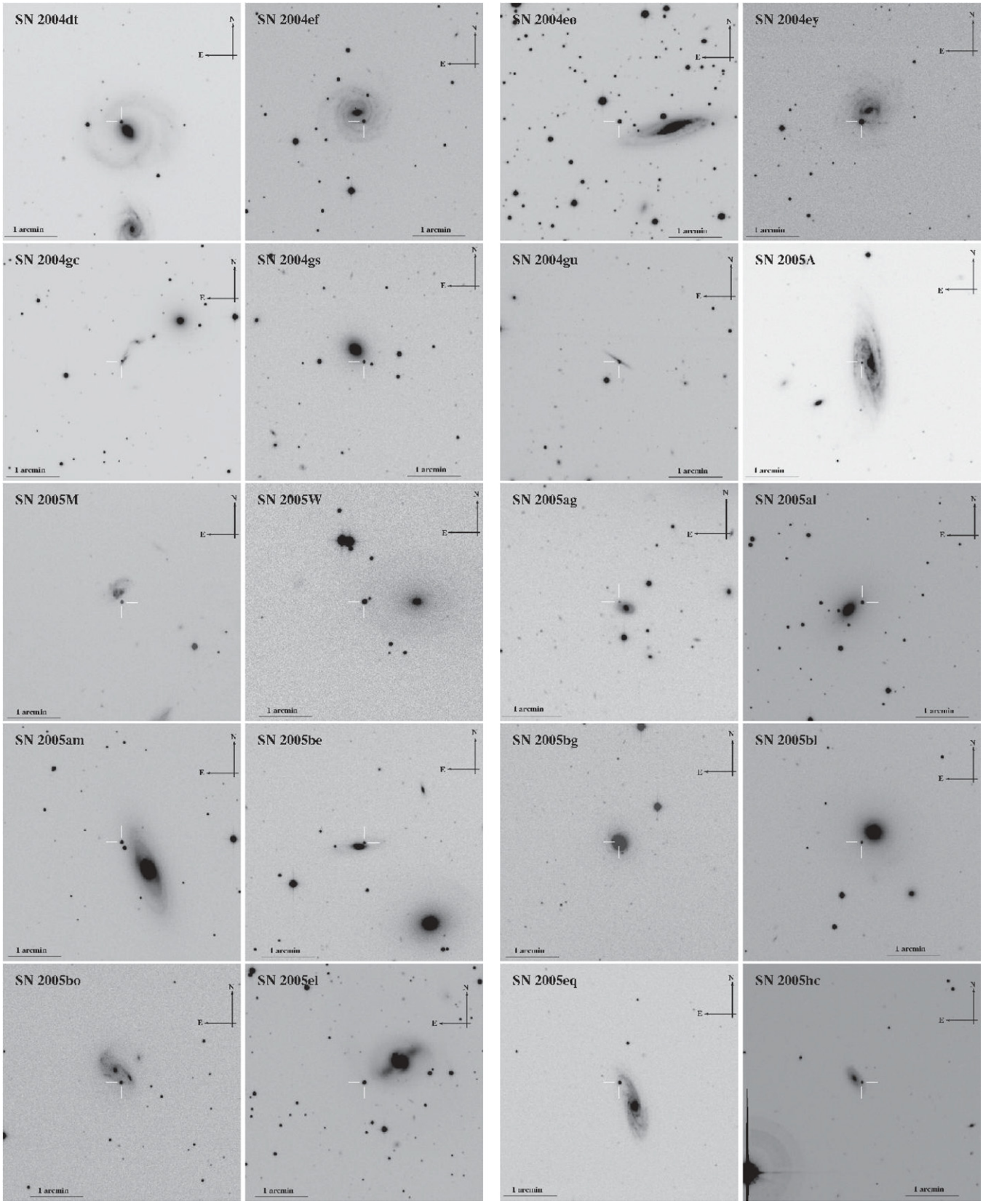

Figure 1. Mosaic of *V*-band CCD images of 35 SNe Ia observed by the CSP.

subtraction, (2) flat-fielding, (3) application of a linearity correction appropriate for the SITe3 CCD, and (4) an exposure-time correction that corrects for a shutter time delay. Both the linearity and exposure-time corrections were monitored frequently during the first three campaigns, and the results are completely consistent with those given in Appendices A and B of H06.

For basic reduction of the near-infrared imaging, we have developed a specific data reduction pipeline (written in C that uses

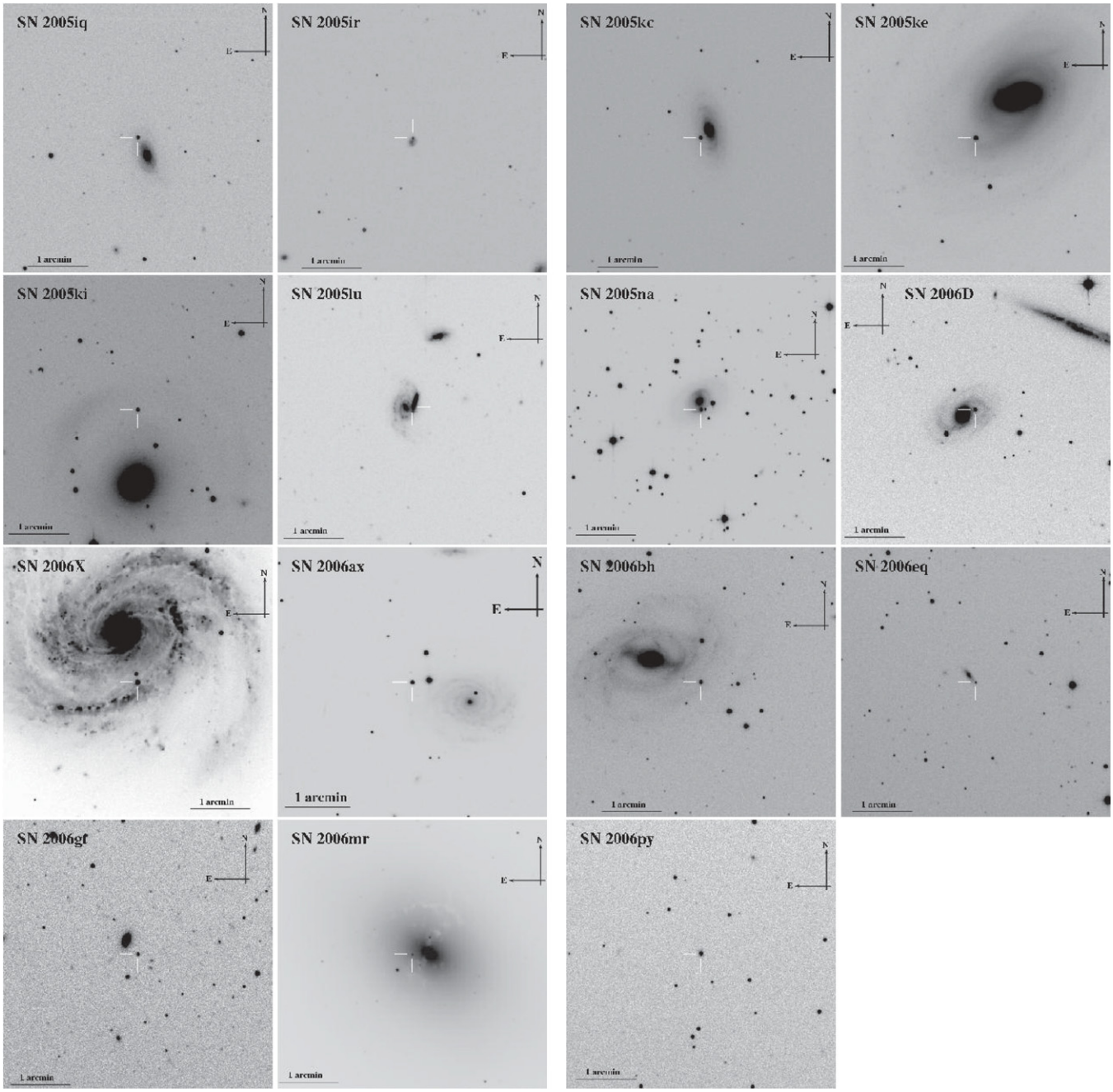

Figure 1. (Continued)

IRAF libraries) for each instrument at LCO. These pipelines apply to each image corrections for detector linearity, electronic bias, pixel-to-pixel variations of the detector's sensitivity, and sky background. During the September–May period, the atmospheric conditions at LCO are typically quite stable. Through the course of the CSP, we found that significant variations in seeing did not normally occur between the individual dithered images. Hence, as a general rule, once all of the dithered images were fully reduced, they were aligned and stacked *without convolving the image quality* to make a master frame which was then used to compute photometry.

3. PHOTOMETRIC SEQUENCES

The brightness of each SN is obtained differentially with respect to a set of local sequence stars. Absolute photometry of each local sequence is derived using observations of photometric standards generally obtained on a minimum of three photometric nights (see Columns 5 and 6 of Table 2). In the optical, we use standards that are in common with both the Landolt (1992) and Smith et al. (2002) catalogs. Aperture photometry of the standard stars is computed using an aperture with a radius of 7″.

To place the instrumental magnitudes of the local sequence stars on the standard Landolt BV and Smith et al. (USNO40) $u'g'r'i'$ photometric systems, we use the transformation Equations (1)–(6) given in H06. Figures 3 and 4 show plots of the extinction and color coefficients employed in these transformation equations, which were derived on photometric nights during the first four CSP campaigns. These figures illustrate the stability of our photometric system, as well as the excellent quality of the LCO site where, during September–May, conditions

Table 2
Photometric/Spectroscopic Properties of the 35 SNe Ia

SN	$\Delta m_{15}(B)$[a] (mag)	Opt. Epochs	NIR Epochs	Opt. Std. Epochs	NIR. Std. Epochs	Spectral Subtype[b]	$t(B_{max})$ (Days)[c]
2004dt	...	48	...	5	1	Normal	+23.6
2004ef	1.39(01)	49	4	23	3	Normal	−1.8
2004eo	1.36(03)	42	9	14	3	Normal	−10.3
2004ey	0.97(01)	33	10	9	4	Normal	−0.8
2004gc	1.09(06)	29	...	7	...	Normal	+11.1
2004gs	1.54(02)	56	12	6	5	Normal	−3.4
2004gu	0.80(04)	31	8	4	3	06gz-like	−3.1
2005A	1.16(06)	37	11	6	7	Normal	+25.4
2005M	0.82(01)	57	18	6	8	91T-like	−0.1
2005W	1.15(06)	22	...	5	...	...	...
2005ag	0.86(01)	46	9	6	3	Normal	+0.4
2005al	1.25(02)	35	8	8	5	Normal	+14.0
2005am	1.45(03)	38	6	8	6	Normal	+7.7
2005be	1.47(08)	13	...	4	...	Normal	+7.2
2005bg	1.02(08)	16	...	3	...	Normal	+2.0
2005bl	1.80(04)	12	...	2	...	91bg-like	−4.6
2005bo	1.30(08)	10	...	3	...	Normal	−1.0
2005el	1.28(02)	26	23	6	8	Normal	−6.4
2005eq	0.78(01)	27	15	6	5	91T-like	−5.4
2005hc	0.91(01)	25	13	6	5	Normal	−5.4
2005iq	1.22(02)	20	12	4	5	Normal	+10.8
2005ir	0.83(09)	14	...	4	...	...	...
2005kc	1.17(02)	13	9	4	4	Normal	+0.83
2005ke	1.69(03)	40	30	6	20	91bg-like	−1.4
2005ki	1.36(02)	47	15	5	3	Normal	−5.8
2005lu	0.88(03)	17	...	3	1	Normal	+12.7
2005na	0.95(02)	27	14	3	5	Normal	+11.7
2006D	1.39(02)	42	17	8	5	Normal	−6.1
2006X	1.02(03)	41	33	6	19	Normal	−6.3
2006ax	0.97(02)	28	19	4	13	Normal	−10.6
2006bh	1.36(01)	25	12	3	8	Normal	+8.2
2006eq	1.66(06)	19	12	4	8	Normal	+26.4
2006gt	1.66(03)	13	10	3	4	91bg-like	−0.3
2006mr	1.71(05)	31	23	4	15	91bg-like	−2.3
2006py	1.02(03)	7	...	3	...	Normal	+16.0

Notes.
[a] Uncertainties are given in parentheses in hundreds of a magnitude.
[b] Most likely spectral subtype as determined by the SNID code (Blondin & Tonry 2007).
[c] Epoch of spectrum (with respect to time of B-band maximum) used to classify spectral type with SNID.

are photometric ∼65% of the time. When determining absolute photometry of the local sequences, we have used the average values of the color coefficients obtained during the first campaign (see Figure 4 of H06). These values differ only slightly from the four-year averages shown in Figure 4. The final magnitudes reported for each sequence star were determined from an average of measurements that were calibrated to standard fields typically on a minimum of three photometric nights.

The color terms shown in Figure 4 can be used to improve our knowledge of the response functions of the CSP optical filters. In Appendix A, we describe such an analysis. In summary, we find that matching the color terms for the BV and $g'r'i'$ filters requires only minor modifications of the bandpasses given in H06. However, the response function of the CSP u' filter clearly differs significantly from that provided in H06.

Absolute photometry of the near-infrared local sequences was calibrated with observations of Persson et al. (1998) standards. Standard Y-band magnitudes of the Persson et al. standards were derived from J- and K_s-band measurements as described by Equation (C2) of H06. As detailed in Appendix B, observations of the A0V star Feige 16 obtained during the course of the CSP

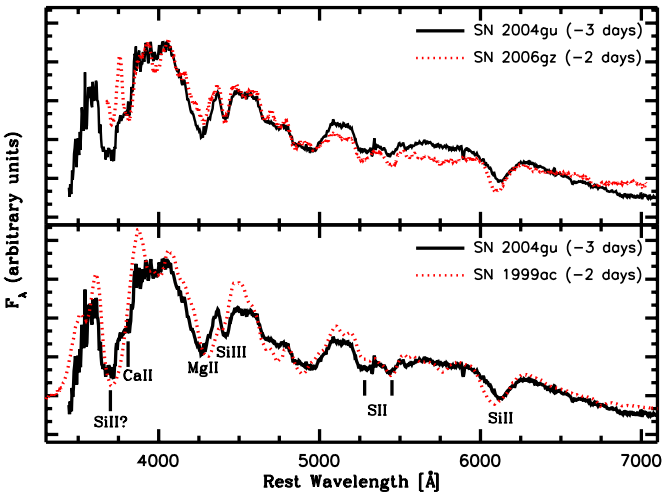

Figure 2. Day −3 spectrum of SN 2004gu (solid line) compared to day −2 spectra of SN 2006gz (bottom panel) and SN 1999ac (bottom panel). Prominent ions are indicated.

(A color version of this figure is available in the online journal.)

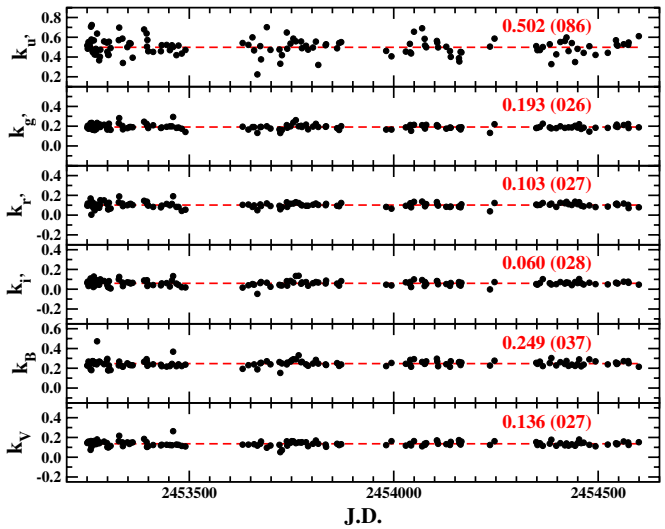

Figure 3. Extinction coefficients for the $u'g'r'i'BV$ filters as a function of time. The average coefficient is plotted with a horizontal line and its numerical value is indicated in each panel along with the rms scatter (in parentheses) expressed in thousandths of a magnitude.

(A color version of this figure is available in the online journal.)

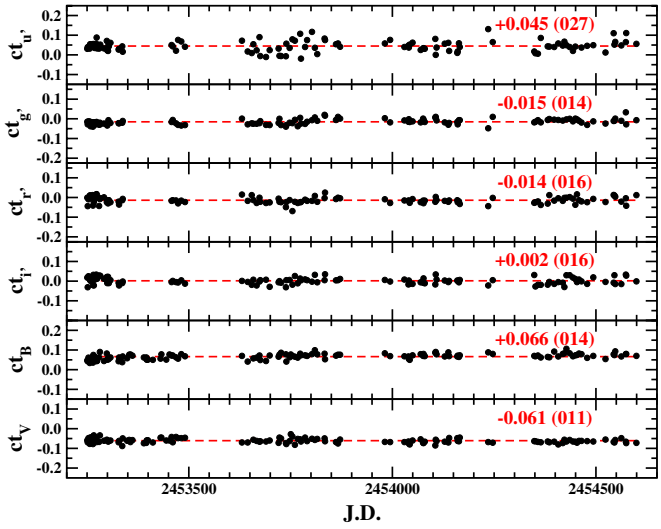

Figure 4. Color coefficients for the $u'g'r'i'BV$ filters as a function of time. The average coefficient is plotted with a horizontal line and its numerical value is indicated in each panel along with the rms scatter (in parentheses) expressed in thousandths of a magnitude.

(A color version of this figure is available in the online journal.)

campaigns confirm that the *Y*-band calibration given in H06 is consistent with the Elias et al. (1982) system, where α Lyrae has 0.00 color. As in H06, we neglect any color term in the near-infrared (see Equations (8)–(11) in H06) since we have been using essentially the same filters employed by Persson et al. to establish the standard system. This assumption will be examined and tested in a future paper.

Final magnitudes of the local sequences in the *standard* system are listed in Table 3. The accompanying uncertainties are weighted averages of the instrumental errors computed from multiple measurements of each sequence star obtained on different photometric nights.

As many of our near-infrared local standards are also included in the Two Micron All Sky Survey (2MASS) catalog[10], we have carried out a comparison of photometry. A total of 984 stars were identified with *J*- and *H*-band measurements in both systems, whereas for K_s we found only 41 stars in common. Generally speaking, the uncertainties in the 2MASS measurements are a factor of ∼2 larger than those in the CSP photometry. Concentrating on the *J* and *H* bands, we find the following mean offsets between the zero points of the CSP and 2MASS magnitudes:

$$J_{\rm CSP} - J_{\rm 2MASS} = 0.010 \pm 0.003 \,{\rm mag},$$
$$H_{\rm CSP} - H_{\rm 2MASS} = 0.043 \pm 0.003 \,{\rm mag}.$$

To determine if there are any significant color terms, we looked for possible correlations of $J_{\rm CSP} - J_{\rm 2MASS}$ and $H_{\rm CSP} - H_{\rm 2MASS}$ versus $(J-H)_{\rm CSP}$. Over the range of color covered by the stars ($0.2 < (J-H)_{\rm CSP} < 0.7$ mag), we obtained the following fits:

$$J_{\rm CSP} - J_{\rm 2MASS} = (-0.045 \pm 0.008) \times (J-H)_{\rm CSP} + (0.035 \pm 0.067)$$
$$H_{\rm CSP} - H_{\rm 2MASS} = (0.005 \pm 0.006) \times (J-H)_{\rm CSP} + (0.038 \pm 0.080).$$

Thus, there is some indication of a small color term in the *J* band, but not in *H*.

[10] http://www.ipac.caltech.edu/2mass/

4. SUPERNOVA PHOTOMETRY

4.1. Host-galaxy Subtraction

Before final photometry of each SN is computed, a template image of the host galaxy is subtracted from each science frame. The templates are obtained a year or more after the last follow-up image with the du Pont Telescope using the same filters employed to take the original science images. By this time, the brightness of the SN has decreased by at least ∼5 mag below the last follow-up measurement. Useful templates are ∼3 mag deeper than the Swope images, and are always obtained under seeing conditions that either exceed or match those of the best science frames.

Although the template and science images are obtained with the same filters, a legitimate concern is whether there is a difference between the global response function of the Swope and du Pont instrument/telescope systems, which could affect the quality of our subtractions. To ascertain if such a problem exists, we compared photometry of the local sequence stars derived from both Swope and du Pont images that were observed during photometric nights. This exercise revealed no indication of any relative color terms. However, in the future, when a more statistically significant sample of template images becomes available, we will revisit this issue.

To perform the galaxy subtraction, the template images are geometrically transformed to each science image, convolved with a two-dimensional kernel function to match the point-spread functions (PSFs), and then scaled in flux. The modified template is then subtracted from the follow-up images around the position of the SN with care taken not to subtract away any local sequence stars. Figure 5 displays two cases of galaxy subtractions where the SN is located in a region with substantial host-galaxy contamination. These examples demonstrate the excellent subtractions that we are able to obtain despite the presence of a significant background. Experiments done by adding a sequence of artificial stars to the template-subtracted images surrounding the location of the SN indicate that in essentially all cases the maximum systematic errors incurred from the template subtractions average < 0.01 mag.

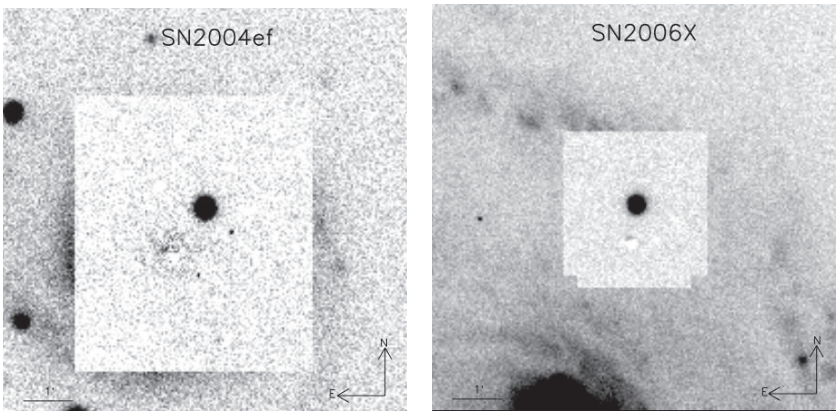

Figure 5. Swope *V*-band CCD images of SN 2004ef (left) and SN 2006X (right) after a template image of the host galaxy was subtracted at the location of each SN.

Table 3
Optical and Near-infrared Photometry of the Local Sequences in the Standard System

Star	α(2000)	δ(2000)	u' (mag)	g' (mag)	r' (mag)	i' (mag)	B (mag)	V (mag)	Y (mag)	J (mag)	H (mag)	K_s (mag)
						2004dt						
01	02:02:09.97	−00:08:42.02	17.480(013)	15.486(009)	14.656(007)	14.259(007)	15.989(008)	15.015(013)	...	...	...	...
02	02:02:10.06	−00:06:49.80	18.876(009)	16.778(003)	16.022(003)	15.771(003)	17.285(004)	16.343(005)	14.998(020)	14.696(020)		14.101(020)
03	02:01:57.62	−00:02:08.23	16.346(008)	15.071(007)	14.633(007)	14.474(008)	15.419(004)	14.786(004)	...	...	...	...
04	02:02:04.30	−00:02:30.68	18.613(007)	16.125(004)	15.070(004)	14.617(004)	16.703(004)	15.549(007)	...	...	...	...
05	02:02:05.35	−00:02:05.48	16.377(009)	15.384(004)	15.185(003)	15.136(003)	15.619(004)	15.243(005)	...	...	...	...
06	02:02:08.16	−00:02:01.70	19.695(015)	16.822(003)	15.486(006)	14.274(010)	17.623(004)	16.082(015)	...	...	...	...
07	02:02:10.50	−00:00:49.75	16.850(016)	15.205(011)			15.655(011)		...	...	...	...
08	02:02:18.90	−00:01:14.13	19.653(191)	17.790(014)	17.114(009)	16.819(011)	18.307(075)	17.427(040)	...	...	...	...
09	02:02:21.70	−00:05:34.74	21.215(041)	20.281(014)	19.812(012)	19.550(021)	20.642(025)	19.950(014)	...	...	...	...
10	02:02:24.08	−00:08:31.14	21.419(085)	18.845(004)	17.536(005)	16.675(004)	19.567(011)	18.118(005)	...	...	...	...

Note. Uncertainties given in parentheses in thousandths of a magnitude correspond to an rms of the magnitudes obtained on at least three photometric nights, with a minimum uncertainty of 0.015 mag for an individual measurement.

(This table is available in its entirety in machine-readable and Virtual Observatory (VO) forms in the online journal. A portion is shown here for guidance regarding its form and content.)

Nevertheless, despite the excellent quality of the template subtractions, it is still possible for the template-subtraction process to introduce a systematic error *at the specific location of the SN*. Such an error could, in principle, lead to a correlated error in the light-curve photometry since the same template is employed in the host-galaxy subtractions for all of the SN images. *We note that even in the ideal case of a perfect subtraction, there will be a correlated error caused by the finite signal-to-noise ratio in the template image.* We have estimated the magnitude of such correlations using the photometry of artificial stars located at fixed positions around the SN, for those cases with the highest background. As explained by Folatelli et al. (2010), we found negligible variations in the light-curve fit parameters and their uncertainties when considering these correlations.

4.2. Photometry

4.2.1. Optical

At this point, our procedure supersedes what was described in H06. Given the non-stellar nature of the spectral energy distribution (SED) of SNe Ia, the conversion of instrumental magnitudes to the *standard* system by application of the color term derived from the photometric standard stars does not guarantee that the SN photometry will actually be on the *standard* system. On the contrary, significant systematic errors can occur between two sets of observations of the same SN put on the same photometric system through application of color terms if the filter response functions are very different (e.g., see Figure 2 in Krisciunas et al. 2003). It is possible to place the SN photometry in the *standard* (or any other desired) photometric system only via application of an additional time-dependent term computed synthetically from template SN spectra, often referred to as an "*S*-correction" (Suntzeff 2000; Stritzinger et al. 2002). We emphasize that this physical effect is important to consider when CSP photometry is to be combined with other optical data sets, *regardless of whether the photometry has been color-corrected*.

A sensible alternative which has been adopted by several other groups (e.g., SN Legacy Survey, ESSENCE, and the CfA Supernova Group) is to not apply the color term and *S*-corrections, and explicitly calculate the SN magnitudes in the *natural* photometric system used for the observations. We thus provide our measurements in the *ugriBV*[11] natural system of the Swope telescope. Photometry in the natural system is the "purest" form of the data and will facilitate in a more transparent way the combination of the CSP photometry with data sets from other groups. Moreover, photometry in this format allows one to easily incorporate improved SN spectral template sequences and/or passbands.

[11] From this point forward, the optical natural photometry is referred to as *ugriBV* as opposed to $u'g'r'i'BV$.

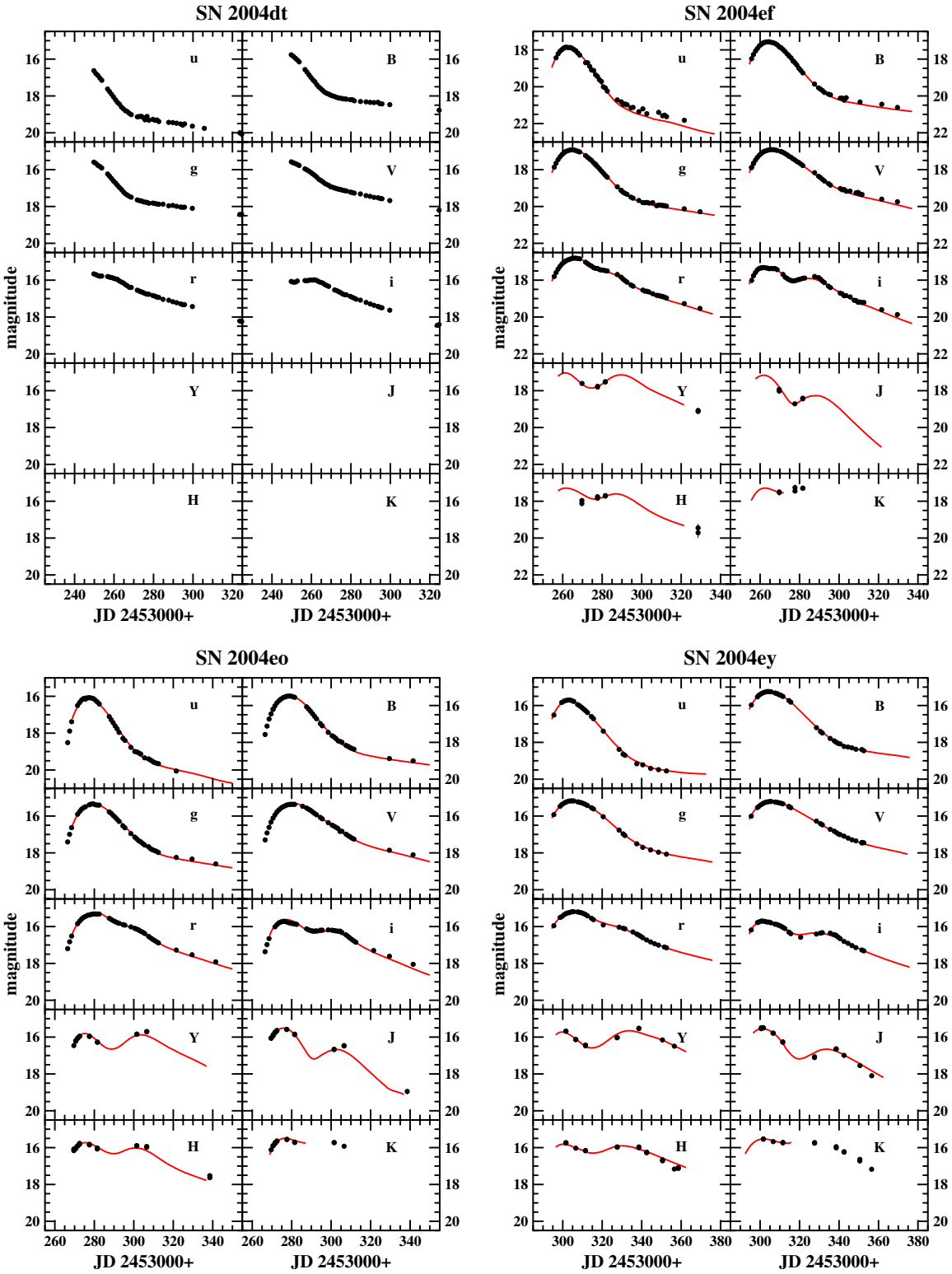

Figure 6. *uBgVriYJHK*$_s$ light curves of the 35 SNe Ia in the natural system of the Swope telescope. Uncertainties in the photometry are smaller than the points, unless shown. The smooth curves show the fits derived with SNOOPy. Note that observations obtained after ∼85 days past *B*-band maximum are not plotted.

(A color version and the complete figure set (35 images) are available in the online journal.)

The specific procedure we have adopted to compute photometry in the natural system is as follows.

1. The magnitudes of the photometric standards given in the catalogs of Landolt (1992) and Smith et al. (2002) are used to calculate new magnitudes of these stars in the natural photometric system of the Swope telescope using the following formulae:

$$u = u'_{\rm std} - ct_u \times (u'_{\rm std} - g'_{\rm std}), \quad (1)$$

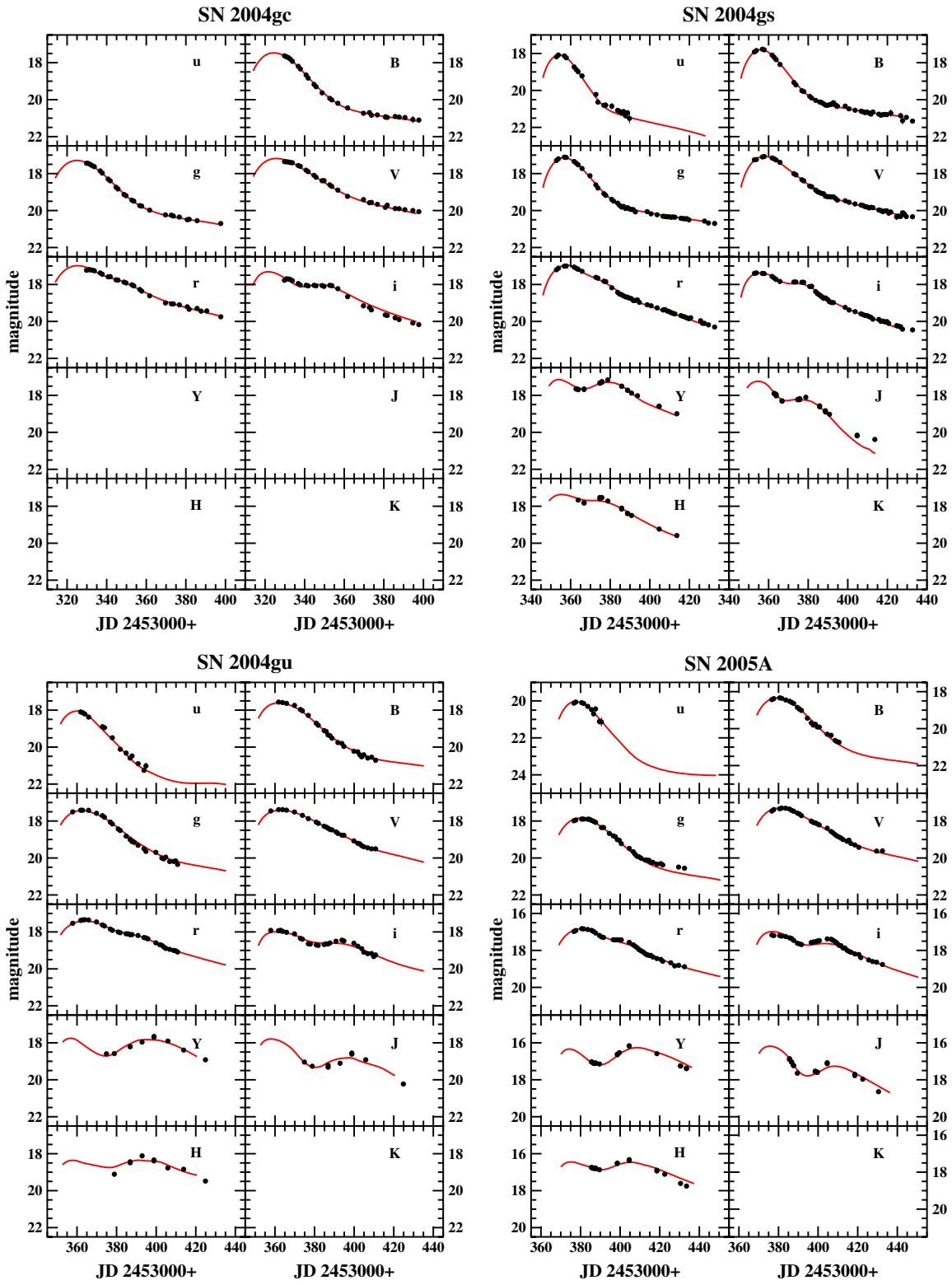

Figure 6. (Continued)

$$g = g'_{\rm std} - ct_g \times (g'_{\rm std} - r'_{\rm std}), \quad (2)$$

$$r = r'_{\rm std} - ct_r \times (r'_{\rm std} - i'_{\rm std}), \quad (3)$$

$$i = i'_{\rm std} - ct_i \times (r'_{\rm std} - i'_{\rm std}), \quad (4)$$

$$B = B_{\rm std} - ct_b \times (B_{\rm std} - V_{\rm std}), \text{ and} \quad (5)$$

$$V = V_{\rm std} - ct_v \times (V_{\rm std} - i'_{\rm std}), \quad (6)$$

where ct_x are the color terms defined in Equations (1)–(6) of H06 (and listed in Figure 4 of H06), and the magnitudes with the "std" subscript are the catalog magnitudes. In constructing our catalog of photometric standards, great care was taken to select stars that cover a broad range in color. Consequently, the optical standards observed by the

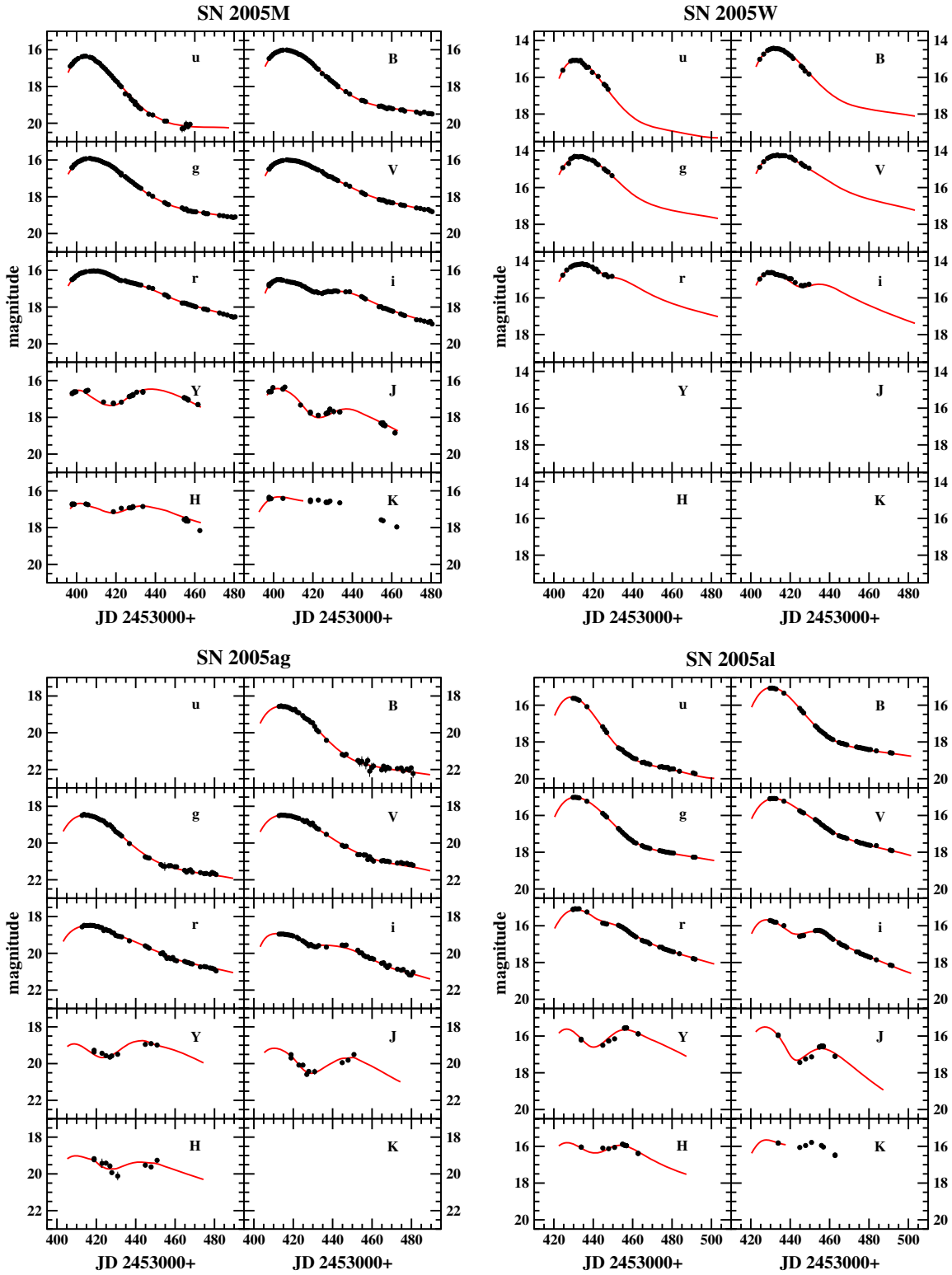

Figure 6. (Continued)

CSP cover a color range of $-0.32 < B - V < 1.60$ mag. For comparison, the vast majority of local sequence stars fall well within this color range.

2. The new catalog of revised photometry is then used to generate natural magnitudes for the local sequence of each SN field from observations obtained on photometric nights. The transformation equation in each band contains an extinction term and a zero point,

$$m_{\rm nat} = m_{\rm inst} - k_i X_i + zp_i,$$

where k_i is the extinction coefficient and X_i is the effective airmass. Note that, unlike Equations (1)–(6) of H06, this equation does not include a color term.

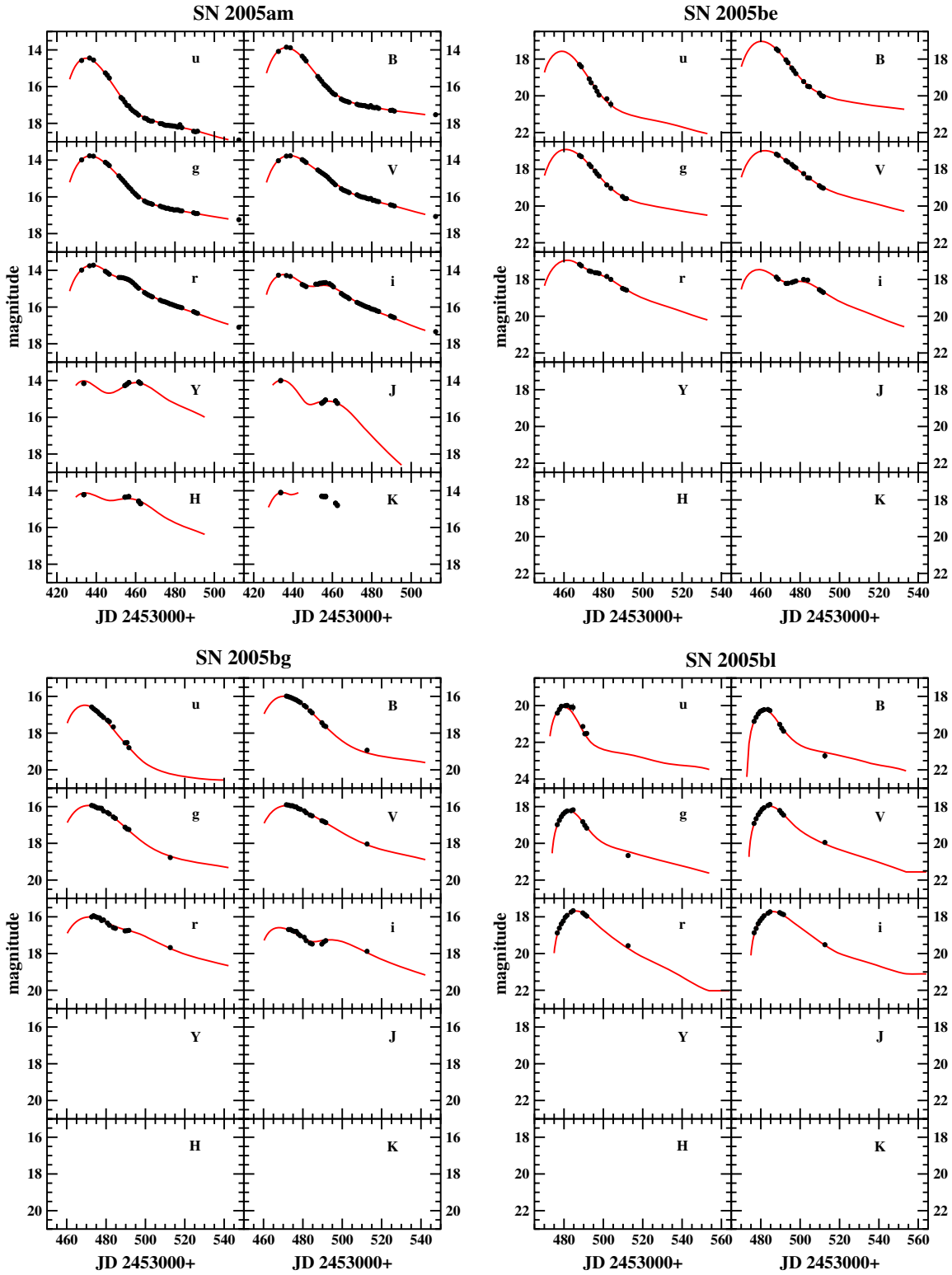

Figure 6. (Continued)

3. Instrumental magnitudes of the local sequence stars and the SN are measured on each galaxy-subtracted frame via PSF fitting. Next, these measurements of the local sequence are compared to the calibrated values in the natural system in order to derive a nightly zero point. This zero point is then used to place the extinction-corrected ($k_i X$) instrumental magnitude of the SN in the natural system.

The treatment of uncertainties is improved with respect to the procedures described in H06. The adopted uncertainty in each magnitude measurement is the result of the sum in quadrature of two components: (a) the uncertainty in the instrumental magnitude, as estimated from the Poisson noise model of the flux of the SN and the surrounding background, and (b) the uncertainty in the fit of the zero point of the image. By

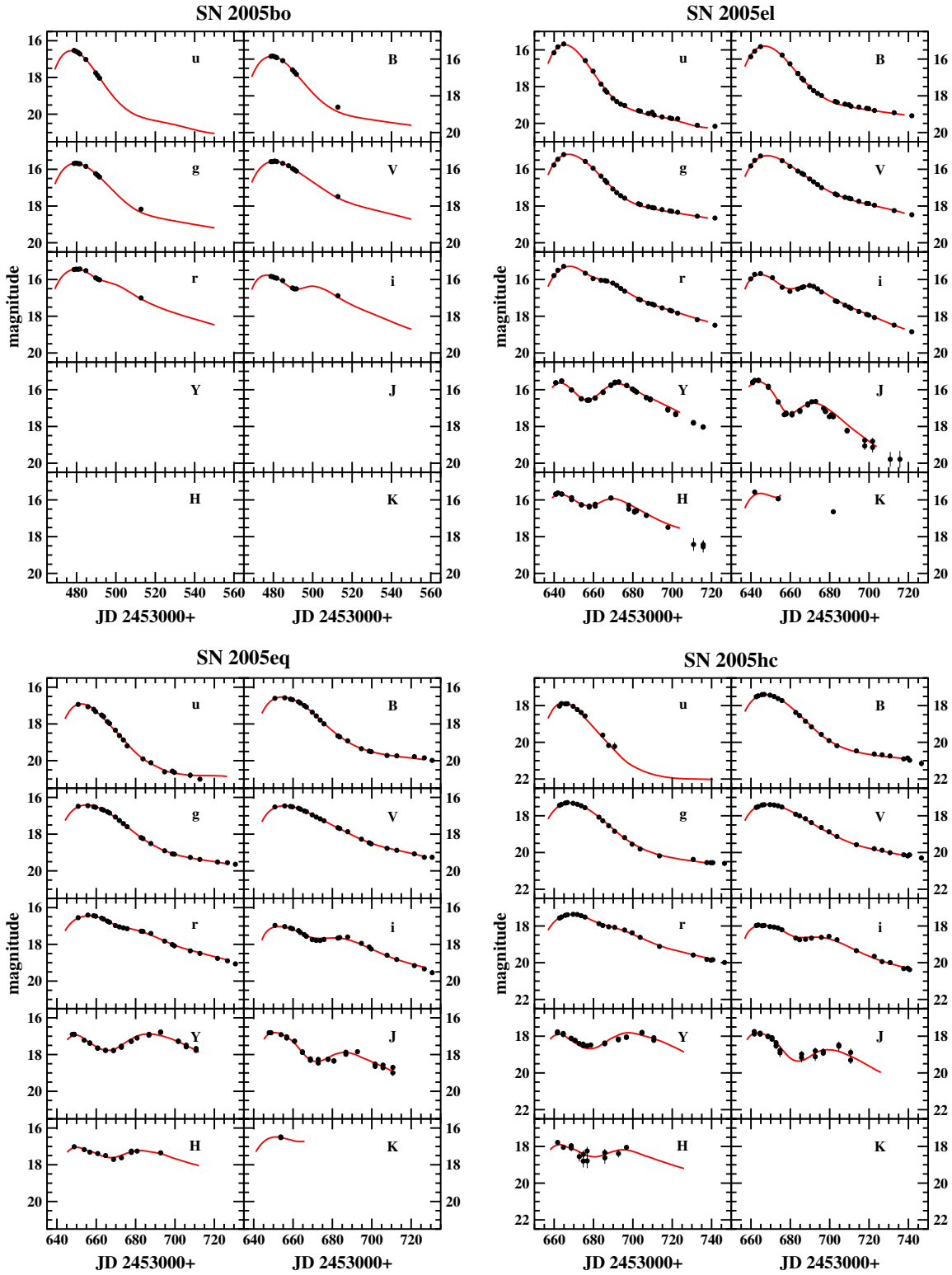

Figure 6. (Continued)

considering the latter term we no longer need to adopt an uncertainty minimum of 0.015 mag, as was done in H06.

4.2.2. Near-infrared

In the near-infrared, we continue to use the procedures described in H06 to measure the final SN magnitudes. As mentioned in Section 3, we neglect any color terms in transforming the measurements made at the Swope and du Pont Telescopes to the Persson et al. (1998) photometric system. Therefore, the local sequence is used only to compute the nightly zero point. Regarding the magnitude uncertainties, we adopt the same procedure as described in the previous section for the optical data: we sum in quadrature the uncertainties in the instrumental magnitude and in the zero-point fit.

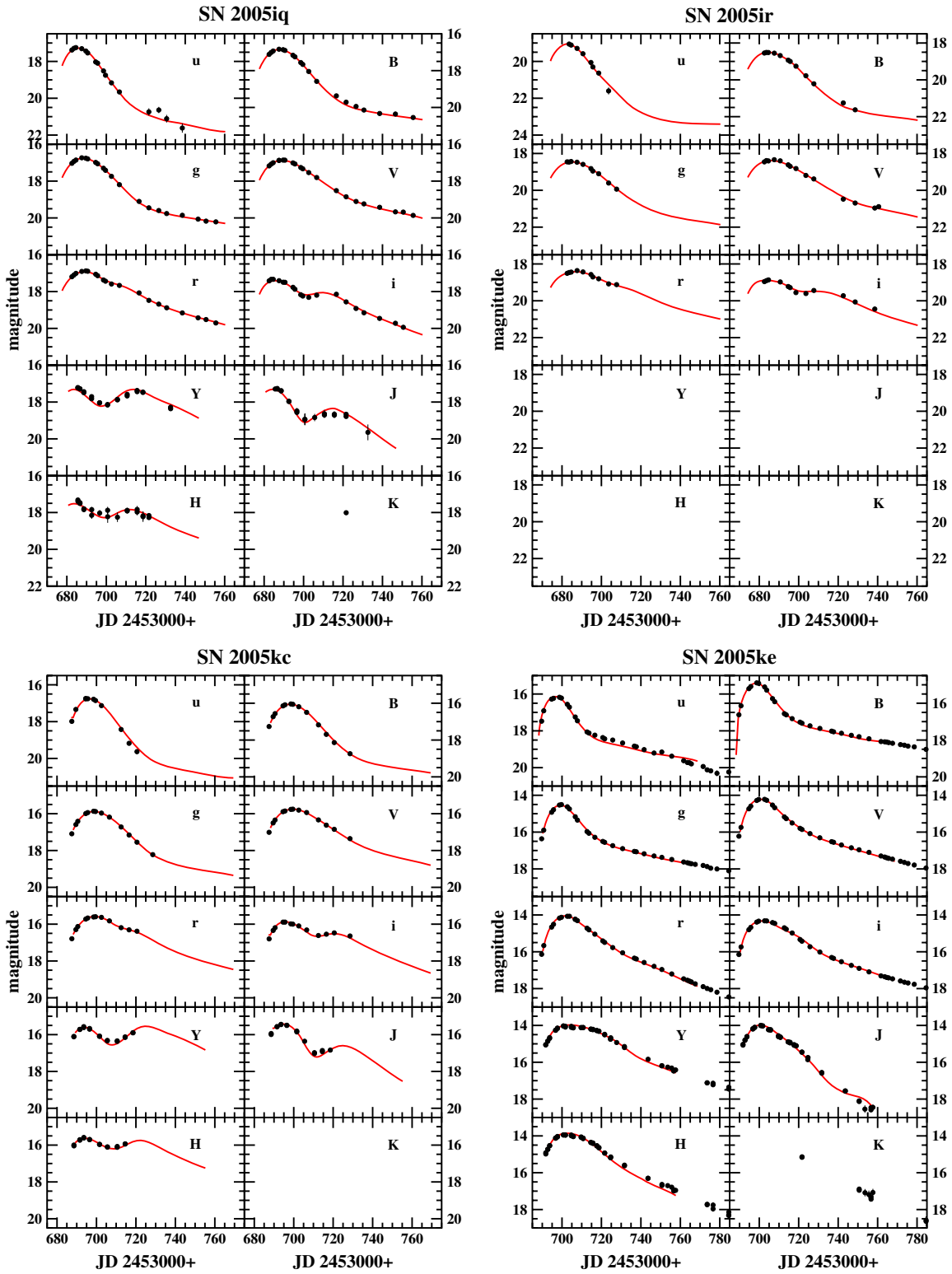

Figure 6. (Continued)

5. FINAL LIGHT CURVES

The final *ugriBV* and $YJHK_s$ magnitudes of the 35 SNe Ia presented in this paper are listed in Tables 4 and 5, respectively. These data are being made available through the NASA/IPAC Extragalactic Database (NED), and can also be accessed on the CSP Web site.[12]

[12] http://www.ociw.edu/csp/

Figure 6 shows the optical and near-infrared light curves, along with fits carried out with SuperNovae in Object-Oriented Python (SNOOPy; C. Burns et al. 2010, in preparation). The template-fitting algorithm implemented in SNOOPy is very simple. We begin by selecting a sample of well-observed CSP SNe that have clear maxima. Using spline fits, we measure the time of B maximum $t_{\max}$, peak magnitude $m_{\max}$ in each filter, and decline-rate parameter $\Delta m_{15}(B)$. Each light curve is

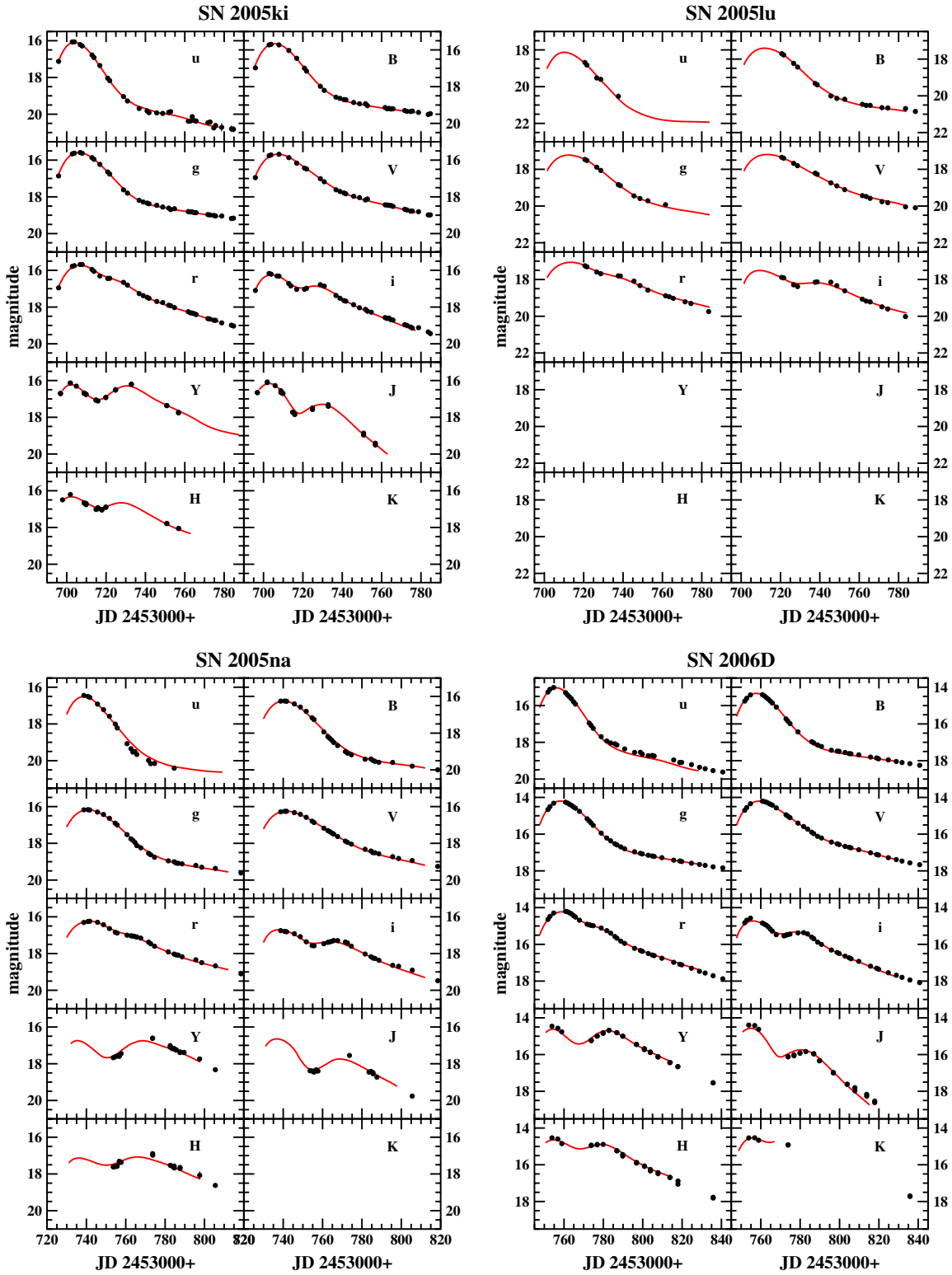

Figure 6. (Continued)

normalized to its peak magnitude and shifted in time such that the B band peaks at epoch $t = 0$. Once this procedure has been done, each data point can be placed in a three-dimensional space based on its epoch, normalized magnitude, and $\Delta m_{15}(B)$. The normalized magnitudes then define a sparsely sampled surface in this space. Generating a template for a particular $\Delta m_{15}(B)$ and set of epochs therefore amounts to interpolating on this surface. For this task, we have chosen a variation of the "gloess" algorithm (B. Madore 2001, private communication), which is a Gaussian-windowed and error-weighted extension of data-smoothing methods outlined by Cleveland (1979), and first implemented by Persson et al. (2004) for fitting Cepheid light curves. A subset of points situated around the interpolation point are selected and assigned weights using an adaptive elliptical Gaussian. These points are then fit with a two-dimensional quadratic using weighted linear least squares. The

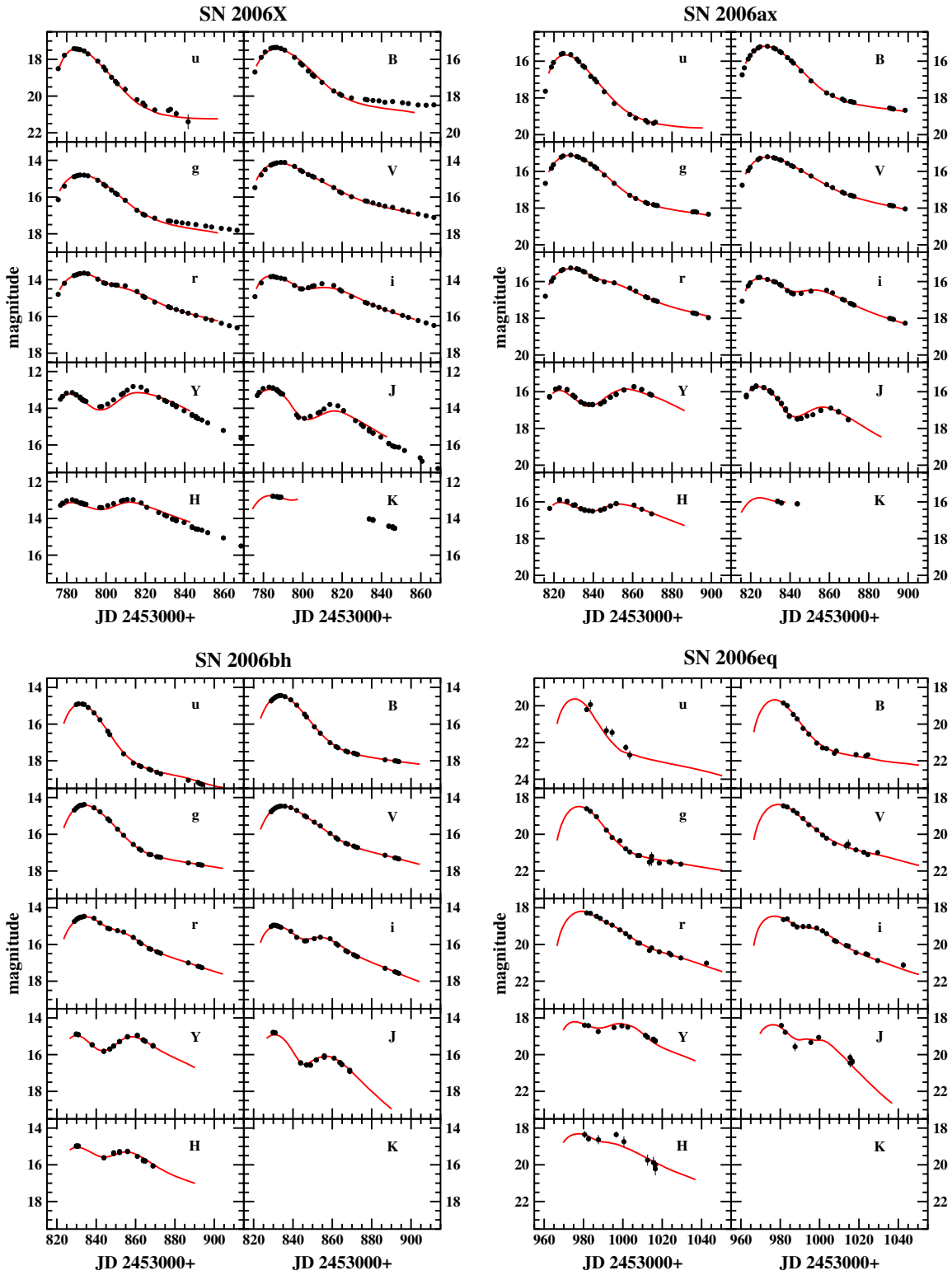

Figure 6. (Continued)

resulting quadratic is then used to interpolate the point of interest.

Given the nonlinear nature of this interpolation algorithm, we use the Levenberg–Marquardt least-squares algorithm to fit the light-curve templates to the data. In doing so, we determine the values of $t_{\max}$, $\Delta m_{15}(B)$, and the peak magnitudes for each filter, as well as a complete covariance matrix for these parameters. The light-curve fitting is performed in flux space. Appendix C gives details of the zero points adopted for the CSP bandpasses.

The $\Delta m_{15}(B)$ values derived from the SNOOPy fits are given in Table 2.[13] From the values of $t_{\max}$, we find that 28 of the 35 SNe have pre-maximum coverage, and for 15 of these, the

[13] In the case of SN 2004dt, the photometry began too late after maximum to obtain a reliable fit with SNOOPy.

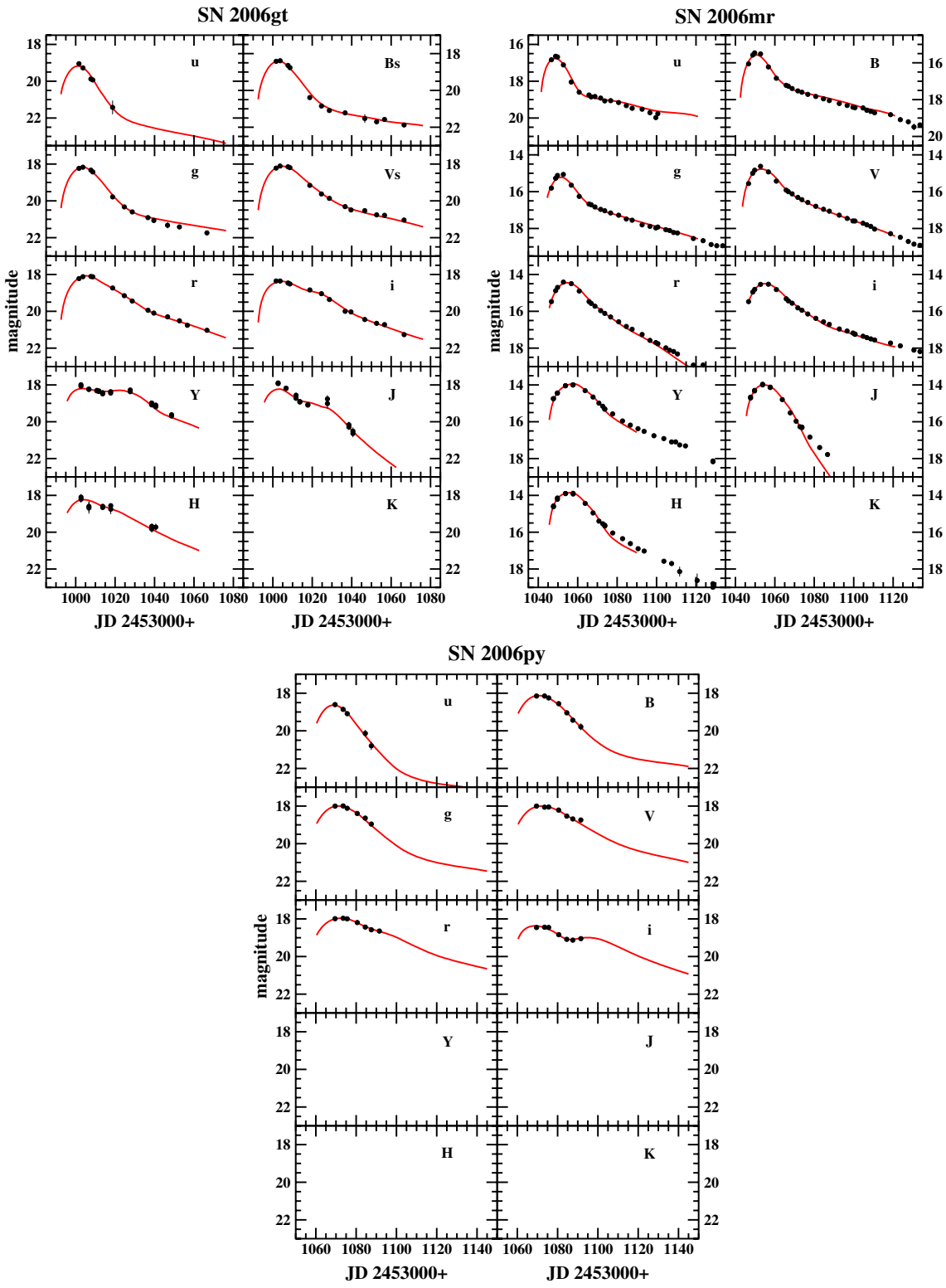

Figure 6. (Continued)

observations began at least 5 days before *B* maximum. In the near-infrared, 17 of the SNe have coverage beginning at or before maximum light, which occurs 3–5 days prior to *B*-band maximum (Folatelli et al. 2010). This was attained for only 4 of the 17 SNe observed during the first campaign, but was achieved for 13 of the 18 SNe observed in the second and third campaigns. This huge improvement is due to the availability of RetroCam beginning in the second campaign. Since its commissioning, RetroCam has become our primary source of near-infrared data, and has allowed the CSP to fulfill its goal of obtaining excellent near-infrared coverage for the majority of the monitored SNe.

6. CONCLUSIONS

In this paper, we have presented the first data release of low-redshift SNe Ia observed by the CSP. The combination of pre-

Table 4
Optical Photometry of 35 SNe Ia in the Swope Natural System

JD 2453000+	u (mag)	g (mag)	r (mag)	i (mag)	B (mag)	V (mag)
			2004dt			
249.77	16.630(013)	15.593(004)	15.660(004)	16.069(006)	15.769(006)	15.576(006)
250.79	16.782(012)	15.661(008)	15.701(007)	16.110(009)	15.848(008)	15.629(009)
251.81	16.886(011)	15.768(008)	15.753(009)	16.110(009)	15.949(009)	15.672(009)
252.85	17.030(011)	15.835(005)	15.786(004)	16.049(007)	16.047(006)	15.719(005)
253.77	17.150(011)	15.910(004)	15.778(004)	···	16.151(013)	15.774(005)
256.72	17.627(009)	16.237(005)	15.803(005)	16.021(007)	16.568(006)	15.960(010)
257.71	17.767(013)	16.355(008)	15.837(010)	16.032(011)	16.705(008)	16.016(009)
258.74	17.913(011)	16.487(005)	15.858(005)	16.008(007)	16.854(007)	16.080(008)
259.76	18.062(011)	16.622(004)	15.901(004)	15.993(005)	16.998(006)	16.159(005)
260.78	18.216(011)	16.732(008)	15.931(009)	15.992(009)	17.132(008)	16.239(008)

Note. Uncertainties given in parentheses in thousandths of a magnitude.

(This table is available in its entirety in machine-readable and Virtual Observatory (VO) forms in the online journal. A portion is shown here for guidance regarding its form and content.)

Table 5
Near-infrared Photometry of 25 SNe Ia

JD 2453000+	Y (mag)	J (mag)	H (mag)	K_s (mag)	Telescope[a]
		2004ef			
269.68	17.606(031)	17.958(048)	18.013(094)	17.515(114)	DUP
277.62	17.769(014)	18.710(049)	17.793(040)	17.391(088)	DUP
281.58	17.518(011)	18.425(023)	17.709(023)	17.294(040)	DUP
328.56	19.095(038)	···	19.553(177)	···	DUP
		2004eo			
269.58	16.459(018)	16.058(007)	16.128(044)	16.117(052)	DUP
270.55	16.210(017)	15.912(028)	16.041(021)	15.899(012)	DUP
271.49	16.058(006)	15.754(018)	15.910(009)	15.757(025)	DUP
272.50	15.961(006)	15.653(013)	15.798(027)	15.648(011)	DUP
277.51	15.958(007)	15.585(005)	15.838(018)	15.553(010)	DUP
281.50	16.276(006)	15.858(012)	16.050(029)	15.713(012)	DUP

Notes. Uncertainties given in parentheses in thousandths of a magnitude.
[a] DUP, SWO, and BAA correspond to the telescopes du Pont, Swope, and Baade, respectively.

(This table is available in its entirety in machine-readable and Virtual Observatory (VO) forms in the online journal. A portion is shown here for guidance regarding its form and content.)

maximum observations, extended coverage, dense sampling, and high signal-to-noise ratio data produces a data set of unprecedented quality. These results will make possible detailed studies of the photometric properties of SNe Ia and serve as a rich resource for comparison with theoretical models. When completed, the CSP data set will constitute a fundamental reference for precise determinations of cosmological parameters such as our own program to measure the i'-band Hubble diagram of SNe Ia to $z \approx 0.7$ (Freedman et al. 2009). The inclusion of the near-infrared data is an important addition since SNe Ia are nearly perfect standard candles at these wavelengths (Krisciunas et al. 2004). In addition, the broad wavelength range covered by the optical and near-infrared observations provides strong leverage for estimating dust extinction in the SN Ia host galaxies (Folatelli et al. 2010).

We thank James Hughes for supporting our network of computers, and the technical staff of the Las Campanas Observatory for its help during many observing nights. C.C. acknowledges José Luis Prieto and Rodrigo Fernández for their continuous support and useful discussions. This material is based upon work supported by the National Science Foundation (NSF) under grant AST–0306969. We also acknowledge support from *Hubble Space Telescope* grant GO-09860.07-A from the Space Telescope Science Institute, which is operated by the Association of Universities for Research in Astronomy, Inc., under NASA contract NAS 5-26555. M.H. acknowledges support provided by NASA through Hubble Fellowship grant HST-HF-01139.01-A, by Fondecyt through grant 1060808, from Centro de Astrofísica FONDAP 15010003, and by the Center of Excellence in Astrophysics and Associated Technologies (PFB 06). G.F., M.H., and F.S. acknowledge support from the Millennium Center for Supernova Science through grant P06-045-F funded by "Programa Bicentenario de Ciencia y Tecnología de CONICYT" and "Programa Iniciativa Científica Milenio de MIDEPLAN." G.F. acknowledges support from Fondecyt through grant 3090004. N.B.S. acknowledges the support of the Mitchell/Heep/Munnerlyn Chair in Astronomy at Texas A&M University, and support though the Dean of the College of Sciences. A.V.F.'s supernova research has been funded by NSF grants AST-0607485 and AST-0908886, as well as by the TABASGO Foundation. KAIT and its ongoing operation were made possible by donations from Sun Microsystems, Inc., the Hewlett-Packard Company, AutoScope Corporation, Lick

Observatory, the NSF, the University of California, the Sylvia & Jim Katzman Foundation, and the TABASGO Foundation.

APPENDIX A

OPTICAL FILTER BANDPASSES

In order to test the CSP optical bandpass response functions given in H06, and to improve these if possible, we employ an approach similar to that of Stritzinger et al. (2005). We start by multiplying the SEDs of the Stritzinger et al. (2005) spectrophotometric atlas of 102 stars with the Johnson B and V passbands from Bessell (1990) and the $u'g'r'i'$ passbands from Smith et al. (2002) to calculate synthetic magnitudes. We derive color terms and zero points by fitting the transformation equations

$$\begin{aligned}
B_{\rm obs} - B_{\rm syn} &= ct_B \times (B_{\rm syn} - V_{\rm syn}) + zp_B,\\
V_{\rm obs} - V_{\rm syn} &= ct_V \times (B_{\rm syn} - V_{\rm syn}) + zp_V,\\
u'_{\rm obs} - u'_{\rm syn} &= ct_{u'} \times (u'_{\rm syn} - g'_{\rm syn}) + zp_{u'},\\
g'_{\rm obs} - g'_{\rm syn} &= ct_{g'} \times (g'_{\rm syn} - r'_{\rm syn}) + zp_{g'},\\
r'_{\rm obs} - r'_{\rm syn} &= ct_{r'} \times (r'_{\rm syn} - i'_{\rm syn}) + zp_{r'}, \text{ and}\\
i'_{\rm obs} - i'_{\rm syn} &= ct_{i'} \times (r'_{\rm syn} - i'_{\rm syn}) + zp_{i'},
\end{aligned}$$

where the "obs" subscript denotes the magnitudes from the Landolt (1992) and Smith et al. (2002) catalogs. If the color terms, ct_X, differ from zero, the bandpasses are shifted in wavelength without changing their shapes. Magnitudes and color terms are recalculated, and the process is repeated until the color terms are consistent with zero.

In B and V, we used the 91 stars contained in both the spectrophotometric atlas and the photometric catalog of Landolt (1992) which are not listed as possible variables. The derived filter shifts of 12.4 ± 3 Å in B and 8.2 ± 4 Å in V are similar to the values of 8.5 Å in B and 6 Åin V found by Stritzinger et al. (2005). The small differences may be due to the inclusion of stars noted as variable or possibly variable by Stritzinger et al. (2005) which were not included in our analysis.

The same analysis was performed for the $u'g'r'i'$ bandpasses. The Smith et al. (2002) u' filter had to be slightly modified: at wavelengths shorter than 3100 Å, the transmission was set to zero because the Stritzinger et al. (2005) spectra begin at 3050 Å. This modification produces photon losses of $< 6\%$. Unfortunately, only 16 of the 102 stars in the Stritzinger et al. (2005) spectrophotometric atlas are included in the Smith et al. (2002) catalog. From this limited sample, the color terms for the g' and r' filters were found to be consistent with zero without applying any shifts. The color terms of the u' and i' filters differed from zero by $\sim 2\sigma$, but given the small sample size, we did not consider this conclusive. Hence, we opted not to apply any shifts to the Smith et al. (2002) $u'g'r'i'$ bandpasses.

Next, we used these revised *standard* bandpasses to calculate synthetic magnitudes in the BV and $u'g'r'i'$ systems for the 91 non-variable stars in the Stritzinger et al. (2005) spectrophotometric atlas. Final adjustment of the zero points for the each bandpass was derived by calculating synthetic magnitudes in BV for α Lyrae and $u'g'r'i'$ for BD+17°4708, and matching these to their standard magnitudes as given by Bessell et al. (1998), Johnson & Morgan (1953), Fukugita et al. (1996), and Smith et al. (2002). Likewise, synthetic magnitudes in the CSP *natural* system were calculated using the BV and *ugri* bandpasses given in H06. Values for the color terms and zero points

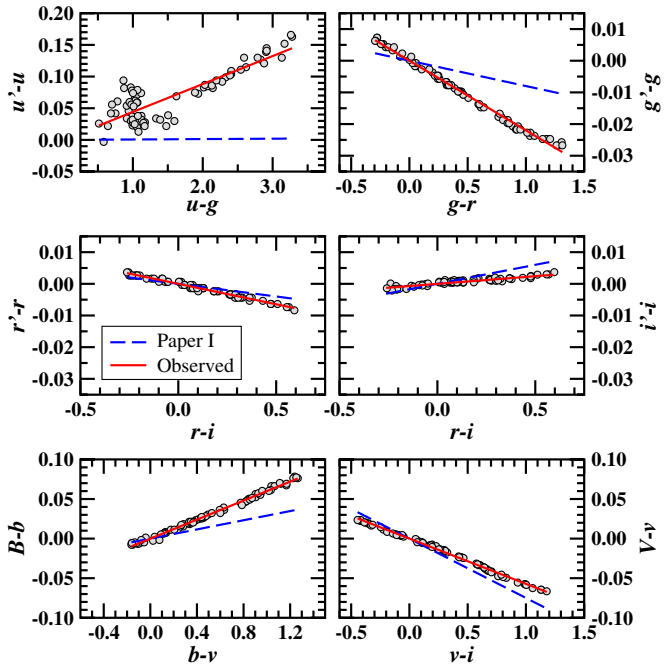

Figure 7. Color transformation terms calculated from synthetic photometry of 91 Landolt standard stars. The dashed blue lines show the predicted color-term slope for the CSP filter response functions given in H06, whereas the solid red lines represent the actual observed slopes. The dots correspond to synthetic photometry of the Landolt standards using the modified CSP *ugriBV* natural bandpasses presented in Appendix A and shown in Figure 8.

(A color version of this figure is available in the online journal.)

were derived from least-squares fits to the transformation equations,

$$\begin{aligned}
B_{\rm std} - B_{\rm nat} &= ct_b \times (B_{\rm nat} - V_{\rm nat}) + zp_b,\\
V_{\rm std} - V_{\rm nat} &= ct_v \times (V_{\rm nat} - i_{\rm nat}) + zp_v,\\
u'_{\rm std} - u_{\rm nat} &= ct_u \times (u_{\rm nat} - g_{\rm nat}) + zp_u,\\
g'_{\rm std} - g_{\rm nat} &= ct_g \times (g_{\rm nat} - r_{\rm nat}) + zp_g,\\
r'_{\rm std} - r_{\rm nat} &= ct_r \times (r_{\rm nat} - i_{\rm nat}) + zp_r, \text{ and}\\
i'_{\rm std} - i_{\rm nat} &= ct_i \times (r_{\rm nat} - i_{\rm nat}) + zp_i,
\end{aligned}$$

where the "std" subscript denotes the synthetic magnitudes in the *standard* system, and the "nat" subscript signifies synthetic magnitudes calculated in the *natural* bandpasses. The natural bandpasses were shifted in wavelength, maintaining their shapes, until the calculated color terms matched the observed ones listed in Figure 4 of H06. As illustrated in Figures 7, excellent results were achieved for the *BV gri* filters by applying the following small shifts: $B = 21.8 \pm 9.7$ Å, $V = 28.6 \pm 17.5$ Å, $g = -14.2 \pm 14.1$ Å, $r = -5.0 \pm 17.0$ Å, and $i = -10.1 \pm 28.6$ Å. The quoted errors for these shifts were derived from matching the formal errors of the observed color terms (see Figure 5).

In the case of the CSP u filter, Figure 7 shows that the observed color term is not at all close to that predicted from the bandpass given in H06. Indeed, even after applying quite large shifts we were unable to match the observed color term. Reasonable agreement could only be achieved after applying a cutoff to the bandpass on the blue side beginning at ~3800 Å and falling to zero at ~3300 Å. This modified u filter bandpass, which must be considered very preliminary at this point, is plotted in Figure 8,

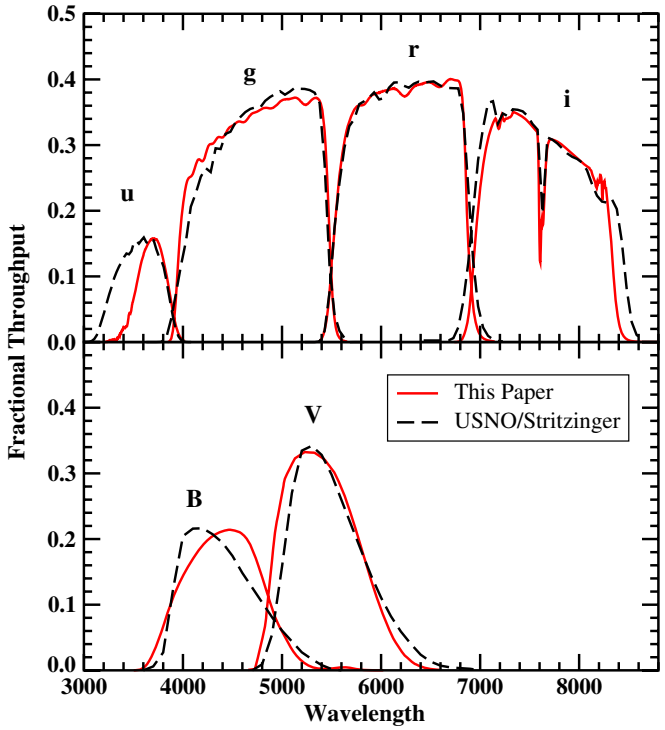

Figure 8. Comparison of revised CSP *ugriBV* natural filter bandpasses (solid lines) with the USNO40 $u'g'r'i'$ and Landolt BV standard bandpasses (Stritzinger et al. 2005) (dashed lines). The USNO40 and Landolt curves have been adjusted to approximately the peak throughputs of the CSP filters.

(A color version of this figure is available in the online journal.)

and the results of the synthetic color-term calculation are shown in Figure 7. We have verified that the transmission of the CSP u filter is consistent with the measurements of the manufacturer, and so this blue cutoff in the bandpass must be produced by the Swope CCD imager, or the telescope optics. We are continuing to investigate this discrepancy so as to provide a more reliable response function for the CSP u bandpass.

APPENDIX B

YJH MEASUREMENTS OF FEIGE 16

According to Landolt (1983, 1992), the A0V star Feige 16 (Feige 1958) has $UBVRI$ colors close to zero. It therefore affords us the opportunity to check the Y-band photometric system presented by Hillenbrand et al. (2002) and in Appendix C of H06. Fifteen measurements of Feige 16 were conducted on six nights with RetroCam. The photometry was computed with respect to several (4–6) Persson et al. (1998) solar-analog standards on each night. We discarded one J and four H measurements as they clearly lay well outside the cluster of values that were averaged with equal weight. Table 6 contains the results, together with the values given by Leggett et al. (2006), transformed according to their prescription, from their Mauna Kea Observatory (MKO) system to the LCO system. We have added 0.015 mag (1σ of the mean) in quadrature to our uncertainties to account for small unknown systematics. For example, although we are treating our JH data as if they were on the system defined by Persson et al. (1998), the fact is that there could be small differences due to the different cameras being used then and now (the filter bandpasses are identical).

The LCO and (transformed) MKO JH measurements agree well, within the stated combined uncertainties. The important result for the calibration of the Y and J bands is that the colors

Table 6
YJH Measurements of Feige 16

System	Y (mag)	J (mag)	H (mag)	Comment
LCO	12.347(016)	12.356(016)	12.334(019)	Measured
MKO	···	12.382(018)	12.359(011)	Transformed to LCO

Note. Uncertainties given in parentheses in thousandths of a magnitude.

Table 7
Photometric Zero Points of CSP Bandpasses

Filter	Zero Point
u	12.400
g	14.432
r	14.136
i	13.687
B	13.669
V	13.774
Y	12.687
J	12.853
H	12.555
K_s	11.967

$Y - J = -0.009$ mag and $Y - H = 0.013$ mag are satisfyingly close to zero. This confirms that our Y-band measurements are indeed on the Elias et al. (1982) system where α Lyrae has 0.00 color. It also confirms the Y–J colors for the Persson et al. (1998) standard stars predicted from model atmospheres presented in Appendix C of H06.

The V magnitude of Feige 16 is 12.400 (Landolt 1983, 1992). Assuming that all the near-infrared colors are actually zero, the average of all the $YJHK_s$ measurements (on the LCO system) is 12.355 mag, indicating that the star may be slightly reddened. If so, $E(B - V) = 0.015$ mag.

APPENDIX C

PHOTOMETRIC ZERO POINTS

The photometric zero point for a filter X with a bandpass response function S_X can be defined as

$$ZP_X = 2.5 \log \left[\int_0^\infty S_X(\lambda)\, F_0(\lambda)\, \frac{\lambda}{hc}\, d\lambda \right] + m_0,$$

where F_0 is the SED of a fiducial source and m_0 is the observed magnitude of this source through filter X. For the purpose of computing photometric zero points for the CSP optical and near-infrared bandpasses, we have adopted the SED of Vega (α Lyr) as presented by Bohlin & Gilliland (2004a). In the following subsections, we outline how the zero points were derived for each bandpass. Table 7 shows the final zero points adopted.

C.1. BV Photometry

The CSP uses the Landolt (1992) standard stars. To derive zero points for our BV filters, we use the SED of Vega as defined by Bohlin & Gilliland (2004a)[14] and the magnitudes adopted by Fukugita et al. (1996): $B_{\rm Vega} = 0.03$ and $V_{\rm Vega} = 0.03$ mag. We convert these magnitudes to the LCO natural system using the color terms from Hamuy et al. (2006). For the V-band transformation, an i' magnitude is needed for Vega. For consistency, we use the Bohlin & Gilliland (2004a) SED for Vega and

[14] This SED can be found at CALSPEC: ftp://ftp.stsci.edu/cdbs/current_calspec/alpha_lyr_stis_004.ascii.

the i' filter function from Fukugita et al. (1996) to compute a synthetic $i'_{\rm Vega} = 0.382$ mag.

C.2. *ugri* Photometry

The CSP uses the Smith et al. (2002) standard stars for the *ugri* photometry, which are tied to the SED of BD+17°4708. *In order to maintain consistency with our choice of the Bohlin & Gilliland (2004a) SED for Vega, we use the SED of BD*+17°4708 *as given by Bohlin & Gilliland (2004b).*[15] For the assumed *ugri* magnitudes of BD+17°4708, we use the values listed in Smith et al. (2002) for the USNO 1.0 m photometric telescope. These magnitudes are then converted to the LCO natural system using the color terms from Hamuy et al. (2006).

C.3. Near-infrared Photometry

Our *Y JHK* photometry uses the standards of Persson et al. (1998), which are tied to the Elias et al. (1982) standards. The Elias et al. (1982) standards are, in turn, tied to Vega. We are therefore on a Vega system and use the Bohlin & Gilliland (2004a) SED. We assume $J_{\rm Vega} = -0.001$, $H_{\rm Vega} = 0.000$, and $K_{\rm Vega} = -0.001$ mag (Cohen et al. 1999), as well as $Y_{\rm Vega} = 0.000$ mag (Hamuy et al. 2006).

REFERENCES

Aldering, G., et al. 2002, Proc. SPIE, 4836, 61
Allen, S. W., et al. 2007, MNRAS, 383, 879
Astier, P., et al. 2006, A&A, 447, 31
Bessell, M. S. 1990, PASP, 102, 1181
Bessell, M. S., Castelli, F., & Plez, B. 1998, PASP, 102, 1181
Blondin, S., & Tonry, J. L. 2007, ApJ, 666, 1024
Bohlin, R. C., & Gilliland, R. L. 2004a, AJ, 127, 3508
Bohlin, R. C., & Gilliland, R. L. 2004b, AJ, 128, 3053
Cleveland, W. S. 1979, J. Am. Stat. Assoc., 74, 829
Cohen, M., Walker, R. G., Carter, B., Hammersley, P., Kidger, M., & Noguchi, K. 1999, AJ, 117, 1864
Elias, J. H., Frogel, J. A., Matthews, K., & Neugebauer, G. 1982, AJ, 87, 1029
Feige, J. 1958, ApJ, 128, 267
Filippenko, A. 2005, in ASP Conf. Ser. 332, The Fate of the Most Massive Stars, ed. R. Humphreys & K. Stanek (San Francisco, CA: ASP), 33
Filippenko, A., Li, W. D., Treffers, R. R., & Modjaz, M. 2001, in ASP Conf. Ser. 246, Small Telescope Astronomy on Global Scales, ed. B. Paczynski, W.-P. Chen, & C. Lemme (San Francisco, CA: ASP), 121
Folatelli, G., et al. 2006, ApJ, 641, 1039
Folatelli, G., et al. 2010, AJ, 139, 120
Freedman, W. L., et al. 2009, ApJ, 704, 1036
Frieman, J. A., et al. 2008, AJ, 135, 338
Fukugita, M., Ichikawa, T., Gunn, J. E., Doi, M., Shimasaku, K., & Schneider, D. P. 1996, AJ, 111, 1748
Giannantonio, T., et al. 2008, Phys. Rev. D, 77, 12350
Hamuy, M., et al. 1996, AJ, 112, 2408
Hamuy, M., et al. 2006, PASP, 118, 2 (H06)
Hicken, M., et al. 2007, ApJ, 669, L17
Hicken, M., et al. 2009, ApJ, 700, 331
Hillenbrand, L. A., Foster, J. B., Persson, S. E., & Matthews, K. 2002, PASP, 114, 708
Jha, S., et al. 2006, AJ, 131, 527
Johnson, H. L., & Morgan, W. W. 1953, ApJ, 117, 313
Krisciunas, K., Phillips, M. M., & Suntzeff, N. B. 2004, ApJ, 602, L81
Krisciunas, K., et al. 2003, AJ, 125, 166
Landolt, A. U. 1983, AJ, 88, 439
Landolt, A. U. 1992, AJ, 104, 340
Leggett, S. K., et al. 2006, MNRAS, 373, 781
Maeda, K., Kawabata, K., Li, W., Tanaka, M., Mazzali, P. A., Hattori, T., Nomoto, K., & Filippenko, A. V. 2009, ApJ, 690, 1745
Perlmutter, S., et al. 1999, ApJ, 517, 565
Persson, S. E., Madore, B. F., Krzeminski, W., Freedman, W. L., Roth, M., & Murphy, D. C. 2004, AJ, 128, 2239
Persson, S. E., Murphy, D. C., Krzeminski, W., Roth, M., & Rieke, M. J. 1998, AJ, 116, 2475
Phillips, M. M. 1993, ApJ, 413, L105
Phillips, M. M., et al. 2006, AJ, 131, 2615
Phillips, M. M., et al. 2007, PASP, 119, 360
Prieto, J. L., et al. 2007, arXiv:0706.4088
Quimby, R. M. 2006, Ph.D. thesis, Univ. Texas
Riess, A. G., et al. 1998, AJ, 116, 1009
Riess, A. G., et al. 1999, AJ, 117, 707
Schweizer, F., et al. 2008, AJ, 136, 1482
Smith, J. A., et al. 2002, AJ, 123, 2121
Stritzinger, M., et al. 2002, AJ, 124, 2100
Stritzinger, M., et al. 2005, PASP, 117, 810
Stritzinger, M., et al. 2009, ApJ, 696, 713
Suntzeff, N. B. 2000, in Cosmic Explosions, ed. S. S. Holt & W. W. Zhang (New York: AIP), 65
Taubenberger, S., et al. 2008, MNRAS, 385, 75
Williams, A. J. 1997, PASA, 14, 208
Wood-Vasey, W. M., et al. 2007, ApJ, 666, 694
Wood-Vasey, W. M., et al. 2008, ApJ, 689, 377

[15] This SED can be found at CALSPEC: ftp://ftp.stsci.edu/cdbs/current_calspec/bd_17d4708_stisnic_002.ascii.